Structured Gaussian Process Models

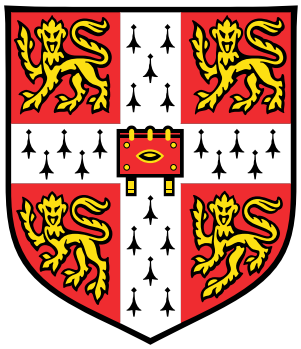

David Kristjanson Duvenaud

Department of Engineering

University of Cambridge

This dissertation is submitted for the degree of

Doctor of Philosophy

Pembroke College

June 2014

I would like to dedicate this thesis to my loving parents ...

Declaration

I hereby declare that except where specific reference is made to the work of others, the contents of this dissertation are original and have not been submitted in whole or in part for consideration for any other degree or qualification in this, or any other University. This dissertation is the result of my own work and includes nothing which is the outcome of work done in collaboration, except where specifically indicated in the text. This dissertation contains less than 65,000 words including appendices, bibliography, footnotes, tables and equations and has less than 150 figures.

David Kristjanson Duvenaud
June 2014

Acknowledgements

And I would like to acknowledge ...

Abstract

This is where you write your abstract ...

Contents

List of Figures

List of Tables

Chapter 1

Introduction

1.1 Regression

1.2 Gaussian process models

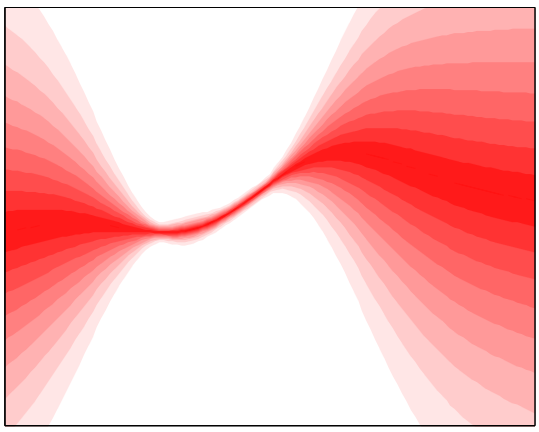

Nothing special about mean

1.3 Latent Variable Models

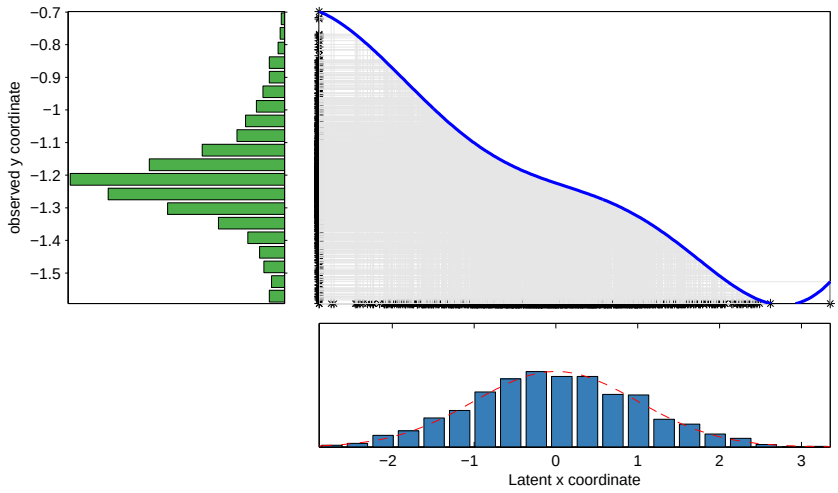

1.4 Derivation of Component Marginal Variance

In this section, we derive the posterior marginal variance and covariance of the additive components of a gp. These formulas let us plot the marginal variance of each component separately. These formulas can also be used to examine the posterior covariance between pairs of components.

Let us assume that our function $\mathbf{f}$ is a sum of two functions, $\mathbf{f}_1$ and $\mathbf{f}_2$, where $\mathbf{f} = \mathbf{f}_1 + \mathbf{f}_2$. If $\mathbf{f}_1$ and $\mathbf{f}_2$ are a priori independent, and $\mathbf{f}_1 \sim \mathrm{gp}(\mu_1, k_1)$ and $\mathbf{f}_2 \sim \mathrm{gp}(\mu_2, k_2)$, then

$$\begin{bmatrix} \mathbf{f}_1 \\ \mathbf{f}_1^\star \\ \mathbf{f}_2 \\ \mathbf{f}_2^\star \\ \mathbf{f} \\ \mathbf{f}^\star \end{bmatrix} \sim \mathcal{N}\left(\begin{bmatrix} \mu_1 \\ \mu_1^\star \\ \mu_2 \\ \mu_2^\star \\ \mu_1 + \mu_2 \\ \mu_1^\star + \mu_2^\star \end{bmatrix}, \begin{bmatrix} \mathbf{k}_1 & \mathbf{k}_1^\star & 0 & 0 & \mathbf{k}_1 & \mathbf{k}_1^\star \\ \mathbf{k}_1^\star & \mathbf{k}_1^{\star\star} & 0 & 0 & \mathbf{k}_1^\star & \mathbf{k}_1^{\star\star} \\ 0 & 0 & \mathbf{k}_2 & \mathbf{k}_2^\star & \mathbf{k}_2 & \mathbf{k}_2^\star \\ 0 & 0 & \mathbf{k}_2^\star & \mathbf{k}_2^{\star\star} & \mathbf{k}_2^\star & \mathbf{k}_2^{\star\star} \\ \mathbf{k}_1 & \mathbf{k}_1^\star & \mathbf{k}_2 & \mathbf{k}_2^\star & \mathbf{k}_1 + \mathbf{k}_2 & \mathbf{k}_1^\star + \mathbf{k}_2^\star \\ \mathbf{k}_1^\star & \mathbf{k}_1^{\star\star} & \mathbf{k}_2^\star & \mathbf{k}_2^{\star\star} & \mathbf{k}_1^\star + \mathbf{k}_2^\star & \mathbf{k}_1^{\star\star} + \mathbf{k}_2^{\star\star} \end{bmatrix} \right) \tag{1.1}$$

where $\mathbf{k}_1 = k_1(\mathbf{X}, \mathbf{X})$ and $\mathbf{k}_1^\star = k_1(\mathbf{X}^\star, \mathbf{X})$.

By the formula for Gaussian conditionals:

$$\mathbf{x}_A | \mathbf{x}B \sim \mathcal{N}(\mu_A + \mathbf{\Sigma}_{AB}\mathbf{\Sigma}_{BB}^{-1}(\mathbf{x}_B - \mu_B), \mathbf{\Sigma}_{AA} - \mathbf{\Sigma}_{AB}\mathbf{\Sigma}_{BB}^{-1}\mathbf{\Sigma}_{BA}), \tag{1.2}$$

we get that the conditional variance of a Gaussian conditioned on its sum with another Gaussian is given by

$$\mathbf{f}_1(\mathbf{x}^\star)|\mathbf{f}(\mathbf{x}) \sim \mathcal{N}\Big(\mu_1^\star + \mathbf{k}_1^{\star\mathsf{T}}(\mathbf{K}_1+\mathbf{K}_2)^{-1}(\mathbf{f}-\mu_1-\mu_2)\,, \tag{1.3}$$

$$\mathbf{k}_1^{\star\star} - \mathbf{k}_1^{\star\mathsf{T}}(\mathbf{K}_1+\mathbf{K}_2)^{-1}\mathbf{k}_1^\star\Big). \tag{1.4}$$

The covariance between the two components, conditioned on their sum is given by:

$$\operatorname{cov}\left[\mathbf{f}_1(\mathbf{x}^\star), \mathbf{f}_2(\mathbf{x}^\star)|\mathbf{f}(\mathbf{x})\right] = -\mathbf{k}_1(\mathbf{x}^\star,\mathbf{x})\left[\mathbf{K}_1(\mathbf{x},\mathbf{x})+\mathbf{K}_2(\mathbf{x},\mathbf{x})\right]^{-1}\mathbf{k}_1(\mathbf{x},\mathbf{x}^\star) \tag{1.5}$$

These formulae express the posterior model uncertainty about different components of the signal, integrating over the possible configurations of the other components.

1.5 Covariance functions

Kernels specify similarity between function values of two objects, not between similarity of objects

Chapter 2

Expressing Structure through Kernels

Kernels specify similarity between function values of two objects, not between similarity of objects.

When modeling functions, encoding known symmetries greatly aids learning and prediction. We demonstrate that in nonparametric regression, many types of symmetry can be enforced through operations on the covariance function. These symmetries can be composed to produce nonparametric priors on functions whose domains have interesting topological structure such as spheres, torii, and Möbius strips. We demonstrate that marginal likeihood an be used to automatically search over such structures.

Joint work with David Reshef, Roger Grosse, Joshua B. Tenenbaum

2.1 Introduction

It is well-known that the properties of the functions we wish to model can be expressed mainly through the covariance function Rasmussen and Williams (2006).

2.2 Expressing Symmetries

In this section, we give recipes for expressing several classes of symmetries. Later, we will show how these can be combined to produce more interesting structures.

Periodicity Given D dimensions, we can enforce rotational symmetry on any subset of the dimensions:

$$f(x) = f(x_i + k\tau_i) \quad \forall k \in \mathbb{Z} \tag{2.1}$$

by the applying a kernel between pairs transformed coordinates $\sin(x), \cos(x)$:

$$k_{\text{periodic}}(x, x') = k(\sin(x), \cos(x), \sin(x'), \cos(x')) \tag{2.2}$$

We can also apply rotational symmetry repeatedy to a single dimension.

Reflective Symmetry along an axis we can enforce the symmetry

$$f(x) = f(-x) \tag{2.3}$$

by the kernel transform

$$\begin{aligned} k_{\text{symm arg1}}(x, x') = k(x, x') + k(x, -x') \\ + k(-x, x') + k(-x, -x') \end{aligned} \tag{2.4}$$

Reflective Symmetry along a diagonal We can enforce symmetry between any two dimensions:

$$f(x, y) = f(y, x) \tag{2.5}$$

by two methods: In the additive method, we transform the kernel by:

$$\begin{aligned} k_{\text{reflect add}}(x, y, x', y') = k(x, y, x', y') \\ + k(x, y, y', x') \\ + k(y, x, x', y') \\ + k(y, x, y', x') \end{aligned} \tag{2.6}$$

or by

$$\begin{aligned} k_{\text{reflect min}}(x, y, x', y') = k(\min(x, y), \max(x, y), \\ \min(x', y'), \max(x', y')) \end{aligned} \tag{2.7}$$

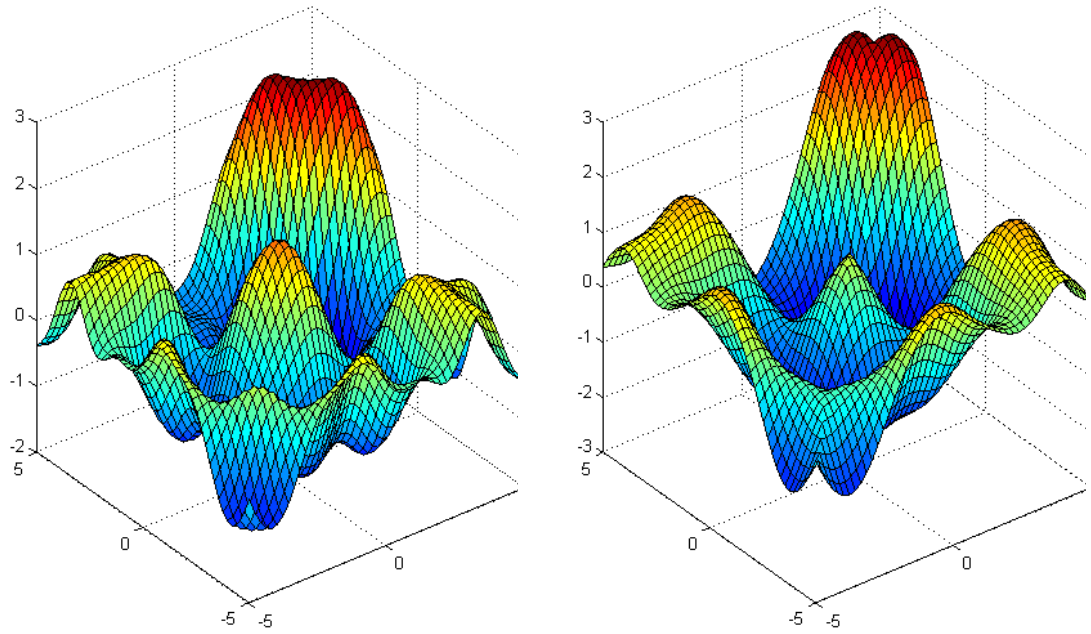

Additive method min method

Fig. 2.1 An illustration of two methods of introducing symmetry: The additive method or the min method. The additive method has half the marginal variance away from $y = x$, but the min method introduces a non-differentiable seam along $y = x$.

however, the second method will in general lead to non-differentiability along $x = y$. Figure 2.1 shows the difference.

Spherical Symmetry We can also enforce that a function expresses the symmetries obeyed by $n - spheres$ by simply transforming a set of $n - 1$ coordinates by:

$$\begin{aligned} x_1 &= \cos(\phi_1) \\ x_2 &= \sin(\phi_1)\cos(\phi_2) \\ x_3 &= \sin(\phi_1)\sin(\phi_2)\cos(\phi_3) \\ &\vdots \\ x_{n-1} &= \sin(\phi_1)\cdots\sin(\phi_{n-2})\cos(\phi_{n-1}) \\ x_n &= \sin(\phi_1)\cdots\sin(\phi_{n-2})\sin(\phi_{n-1}) \end{aligned} \tag{2.8}$$

?

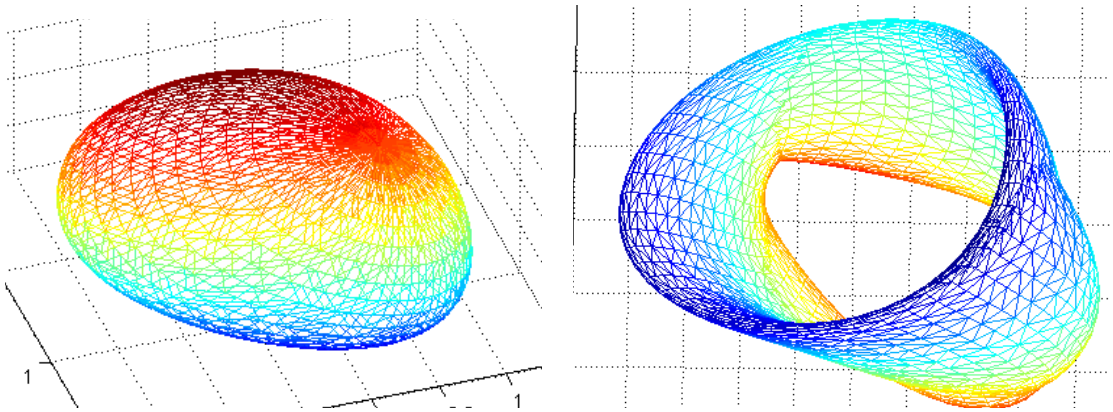

Spheroid Toroid

Fig. 2.2 Generating 2D manifolds with different topological structures. By enforcing that the functions mapping from $\mathbb{R}^2$ to $\mathbb{R}^3$ obey the appropriate symmetries, the surfaces created have the corresponding topologies (ignoring self-intersections).

2.2.1 Parametric embeddings

In general, we can always enforce the symmetries obeyed by a given surface by finding a parametric embedding to that surface. However, it is not clear how to do this in general without introducing unnecessary

2.3 How to generate 3D shapes with a given topology

First create a mesh in 2d. Then draw 3 independent functions from a GP prior with the relevant symmetries encoded in the kernel. Then, map the 2d points making up the mesh through those 3 functions to get the 3D coordinates of each point on the mesh.

This is similar in spirit to the GP-LVM model **?**, which learns an embedding of the data into a low-dimensional space, and constructs a fixed kernel structure over that space.

2.3.1 Möbius strips

A prior on functions on Möbius strips can be achieved fairly easily. We simply need to enforce the following symmetries:

$$f(x, y) = f(x, y + k_y\tau) \quad \forall k_y \in \mathbb{Z} \tag{2.9}$$

$$f(x, y) = f(x + k_x\tau, y) \quad \forall k_x \in \mathbb{Z} \tag{2.10}$$

$$f(x, y) = f(y, x) \tag{2.11}$$

If we imagine moving along a Möbius strip, that is equivalent to moving along a diagonal in the function generated. Figure 2.3 shows this. The second example is doesn't resemble a typical Möbius strip because the edge of the mobius strip is in a geometric circle. This kind of embedding is resembles the Sudanese Möbius strip [cite].

Another classic example of a function living on a Mobius strip is the auditory quality of 2-note intervals. The harmony of a pair of notes is periodic (over octaves) for each note, and the

2.4 Examples

2.4.1 Computing molecular energies

Figure 2.4 gives one example of a function which obeys the same symmetries as a Möbius strip, in some subsets of its arguments.

2.4.2 Translation invariance in images

Most models of images are invariant to spatial translations [cite convolution nets]. Similarily, most models of sounds are also invariant to translation through time.

Note that this sort of translational invariance is completely distinct from the stationarity properties of kernels used in Gaussian process priors. A stationary kernel implies that the prior is invariant to translations of the entire training and test set.

We are discussing here a discretized input space (into pixels or the audio equivalent), where the input vectors have one dimension for every pixel. We are interested in creating

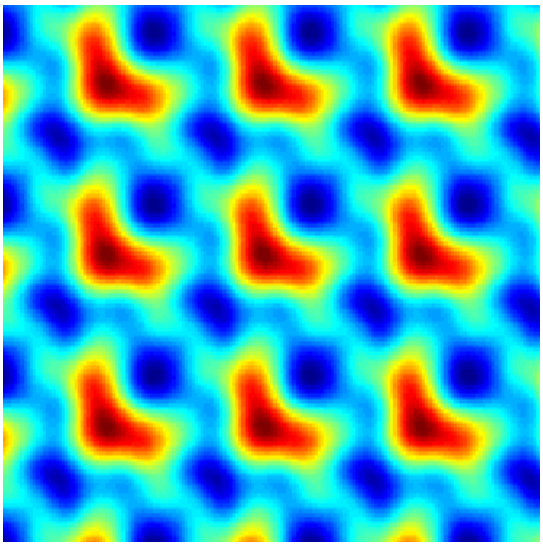

Funcion a Möbius strip

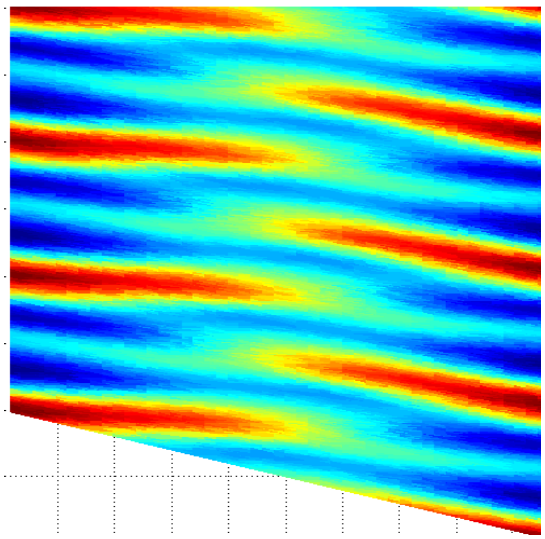

Zoom in along diagonal

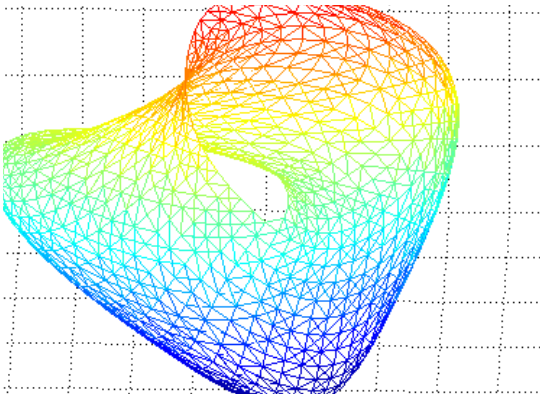

Möbius strip

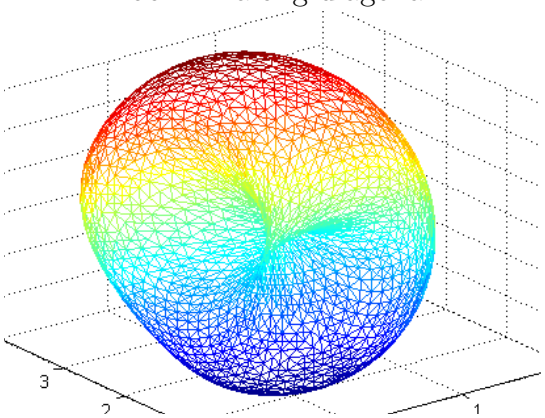

Sudanese Möbius strip

Fig. 2.3 Generating 2D manifolds with different topological structures. By enforcing that the functions mapping from $\mathbb{R}^2$ to $\mathbb{R}^3$ obey the appropriate symmetries, the surfaces created have the corresponding topologies (ignoring self-intersections).

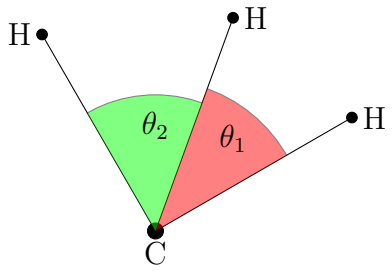

Fig. 2.4 An example of a function expressing the same symmetries as a Mobius strip in two of its arguments. The energy of a molecular configuration $f(\theta_1, \theta_2)$ depends only on the relative angles between atoms, and because each atom is indistiguishable, is invariant to permuting the atoms.

priors on functions that are invariant to shifting a signal along its pixels:

$$f\left(\quad\right) = f\left(\quad\right) \tag{2.12}$$

Translational invariance in this setting is equivalent to symmetries between dimensions in the input space.

This prior can be achieved in one dimension by using the following kernel transformation:

$$k\left((x_1, x_2, \ldots, x_D), (x'_1, x'_2, \ldots, x'_D)\right) = \sum_{i=1}^{D} \prod_{j=1}^{D} k(x_j, x'_{i+j \bmod D}) \tag{2.13}$$

Edge effects can be handled either by wrapping the image around, or by padding it with zeros.

Convolution The resulting kernel could be called a *discrete convolution kernel*. For an image with R, C rows and columns, it can also be written as:

$$k_{\text{conv}}\left((x_{11}, x_{12}, \ldots, x_{RC}), (x'_{11}, x'_{12}, \ldots, x'_{RC})\right) = \sum_{i=-L}^{L} \sum_{j=-L}^{L} k\left(\mathbf{x}, T_{ij}(\mathbf{x}')\right) \tag{2.14}$$

where $T_{ij}(\mathbf{x})$ is the operator which replaces each x_{mn} with $x_{m+i,n+j}$. Thus we are simply defining the covariance between two images to be the sum of all covariances between all relative translations of the two images. We can also normalize the kernel by pre-multiplying it with $\sqrt{k_{\text{conv}}(\mathbf{x},\mathbf{x})k_{\text{conv}}(\mathbf{x}',\mathbf{x}')}$.

Is there a pathology of the additive construction that appears in the limit?

2.4.3 Max-pooling

What we'd really like to do is a max-pooling operation. However, in general, a kernel which is the max of other kernels is not PSD [put counterexample here?]. Is the max over co-ordinate switching PSD?

2.5 Related Work

Invariances in Gaussian processes **?** show that, for Gaussian processes, with probability one, $f(\mathbf{x}) = f(T(\mathbf{x}))$ if and only if $k(x,x') = k(x,T(x'))$.

Structure discovery **?** learned the structural form of a graph used to model human similarity judgments. Examples of graphs included planes, trees, and cylinders. Some of their discrete graph structures have continous analogues in our own space; e.g. $\text{SE}_1 \times \text{SE}_2$ and $\text{SE}_1 \times \text{Per}_2$ can be seen as mapping the data to a plane and a cylinder, respectively.

Chapter 3

Additive Gaussian Processes

In this chapter, we introduce a Gaussian process model of functions which are *additive*. An additive function is one which decomposes into a sum of low-dimensional functions, each depending on only a subset of the input variables. Additive GPs generalize both Generalized Additive Models, and the standard GP models which use squared-exponential kernels. Hyperparameter learning in this model can be seen as Bayesian Hierarchical Kernel Learning (HKL). We introduce an expressive but tractable parameterization of the kernel function, which allows efficient evaluation of all input interaction terms, whose number is exponential in the input dimension. The additional structure discoverable by this model results in increased interpretability, as well as state-of-the-art predictive power in regression tasks.

3.1 Introduction

Most statistical regression models in use today are of the form: $g(y) = f(x_1) + f(x_2) + \cdots + f(x_D)$. Popular examples include logistic regression, linear regression, and Generalized Linear ModelsNelder and Wedderburn (1972). This family of functions, known as Generalized Additive Models (GAM)Hastie and Tibshirani (1990), are typically easy to fit and interpret. Some extensions of this family, such as smoothing-splines ANOVA Wahba (1990), add terms depending on more than one variable. However, such models generally become intractable and difficult to fit as the number of terms increases.

At the other end of the spectrum are kernel-based models, which typically allow the response to depend on all input variables simultaneously. These have the form: $y = f(x_1, x_2, \ldots, x_D)$. A popular example would be a Gaussian process model using a squared-exponential (or Gaussian) kernel. We denote this model as SE-GP. This model

is much more flexible than the GAM, but its flexibility makes it difficult to generalize to new combinations of input variables.

In this paper, we introduce a Gaussian process model that generalizes both GAMs and the SE-GP. This is achieved through a kernel which allow additive interactions of all orders, ranging from first order interactions (as in a GAM) all the way to Dth-order interactions (as in a SE-GP). Although this kernel amounts to a sum over an exponential number of terms, we show how to compute this kernel efficiently, and introduce a parameterization which limits the number of hyperparameters to $O(D)$. A Gaussian process with this kernel function (an additive GP) constitutes a powerful model that allows one to automatically determine which orders of interaction are important. We show that this model can significantly improve modeling efficacy, and has major advantages for model interpretability. This model is also extremely simple to implement, and we provide example code.

We note that a similar breakthrough has recently been made, called Hierarchical Kernel Learning (HKL)Bach (2009). HKL explores a similar class of models, and sidesteps the possibly exponential number of interaction terms by cleverly selecting only a tractable subset. However, this method suffers considerably from the fact that cross-validation must be used to set hyperparameters. In addition, the machinery necessary to train these models is immense. Finally, on real datasets, HKL is outperformed by the standard SE-GP Bach (2009).

3.2 Gaussian Process Models

Gaussian processes are a flexible and tractable prior over functions, useful for solving regression and classification tasksRasmussen and Williams (2006). The kind of structure which can be captured by a GP model is mainly determined by its *kernel*: the covariance function. One of the main difficulties in specifying a Gaussian process model is in choosing a kernel which can represent the structure present in the data. For small to medium-sized datasets, the kernel has a large impact on modeling efficacy.

Figure 4.2 compares, for two-dimensional functions, a first-order additive kernel with a second-order kernel. We can see that a GP with a first-order additive kernel is an example of a GAM: Each function drawn from this model is a sum of orthogonal one-dimensional functions. Compared to functions drawn from the higher-order GP, draws from the first-order GP have more long-range structure.

We can expect many natural functions to depend only on sums of low-order interac-

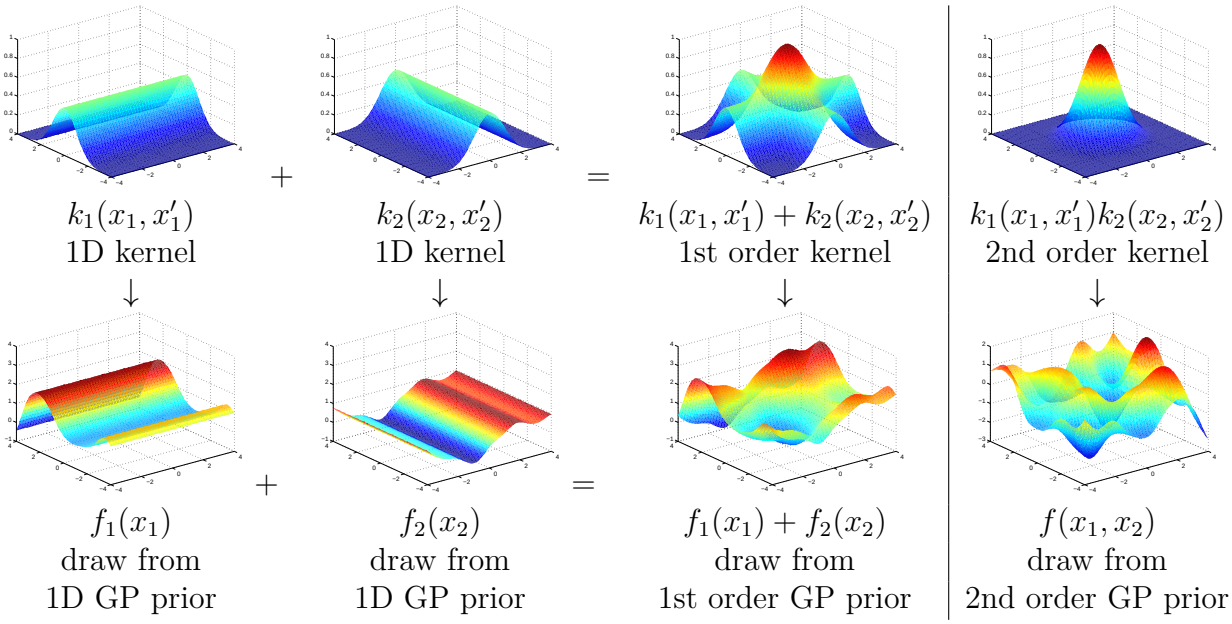

Fig. 3.1 A first-order additive kernel, and a product kernel. Left: a draw from a first-order additive kernel corresponds to a sum of draws from one-dimensional kernels. Right: functions drawn from a product kernel prior have weaker long-range dependencies, and less long-range structure.

tions. For example, the price of a house or car will presumably be well approximated by a sum of prices of individual features, such as a sun-roof. Other parts of the price may depend jointly on a small set of features, such as the size and building materials of a house. Capturing these regularities will mean that a model can confidently extrapolate to unseen combinations of features.

3.3 Additive Kernels

We now give a precise definition of additive kernels. We first assign each dimension $i \in \{1 \dots D\}$ a one-dimensional *base kernel* $k_i(x_i, x_i')$. We then define the first order, second order and nth order additive kernel as:

$$k_{add_1}(\mathbf{x}, \mathbf{x}') = \sigma_1^2 \sum_{i=1}^{D} k_i(x_i, x_i') \tag{3.1}$$

$$k_{add_2}(\mathbf{x}, \mathbf{x}') = \sigma_2^2 \sum_{i=1}^{D} \sum_{j=i+1}^{D} k_i(x_i, x_i') k_j(x_j, x_j') \tag{3.2}$$

$$k_{add_n}(\mathbf{x}, \mathbf{x}') = \sigma_n^2 \sum_{1 \le i_1 < i_2 < \ldots < i_n \le D} \left[\prod_{d=1}^{n} k_{i_d}(x_{i_d}, x_{i_d}') \right] \tag{3.3}$$

where D is the dimension of our input space, and σ_n^2 is the variance assigned to all nth order interactions. The nth covariance function is a sum of $\binom{D}{n}$ terms. In particular, the Dth order additive covariance function has $\binom{D}{D} = 1$ term, a product of each dimension's covariance function:

$$k_{add_D}(\mathbf{x}, \mathbf{x}') = \sigma_D^2 \prod_{d=1}^{D} k_d(x_d, x_d') \tag{3.4}$$

In the case where each base kernel is a one-dimensional squared-exponential kernel, the Dth-order term corresponds to the multivariate squared-exponential kernel:

$$k_{add_D}(\mathbf{x}, \mathbf{x}') = \sigma_D^2 \prod_{d=1}^{D} k_d(x_d, x_d') = \sigma_D^2 \prod_{d=1}^{D} \exp\left(-\frac{(x_d - x_d')^2}{2l_d^2}\right) = \sigma_D^2 \exp\left(-\sum_{d=1}^{D} \frac{(x_d - x_d')^2}{2l_d^2}\right) \tag{3.5}$$

also commonly known as the Gaussian kernel. The full additive kernel is a sum of the additive kernels of all orders.

3.3.1 Parameterization

The only design choice necessary in specifying an additive kernel is the selection of a one-dimensional base kernel for each input dimension. Any parameters (such as length-scales) of the base kernels can be learned as usual by maximizing the marginal likelihood of the training data.

In addition to the hyperparameters of each dimension-wise kernel, additive kernels are equipped with a set of D hyperparameters $\sigma_1^2 \ldots \sigma_D^2$ controlling how much variance we assign to each order of interaction. These "order variance" hyperparameters have a useful interpretation: The dth order variance hyperparameter controls how much of the target function's variance comes from interactions of the dth order. Table 3.1 shows examples of normalized order variance hyperparameters learned on real datasets.

On different datasets, the dominant order of interaction estimated by the additive model varies widely. An additive GP with all of its variance coming from the 1st order is equivalent to a GAM; an additive GP with all its variance coming from the Dth order is equivalent to a SE-GP.

Because the hyperparameters can specify which degrees of interaction are important, the additive GP is an extremely general model. If the function we are modeling is decomposable into a sum of low-dimensional functions, our model can discover this fact and exploit it (see Figure 3.5) . If this is not the case, the hyperparameters can specify a suitably flexible model.

Table 3.1 Relative variance contribution of each order in the additive model, on different datasets. Here, the maximum order of interaction is set to 10, or smaller if the input dimension less than 10. Values are normalized to sum to 100.

Order of interaction	1st	2nd	3rd	4th	5th	6th	7th	8th	9th	10th
pima	0.1	0.1	0.1	0.3	1.5	**96.4**	1.4	0.0		
liver	0.0	0.2	**99.7**	0.1	0.0	0.0				
heart	**77.6**	0.0	0.0	0.0	0.1	0.1	0.1	0.1	0.1	22.0
concrete	**70.6**	13.3	13.8	2.3	0.0	0.0	0.0	0.0		
pumadyn-8nh	0.0	0.1	0.1	0.1	0.1	0.1	0.1	**99.5**		
servo	**58.7**	27.4	0.0	13.9						
housing	0.1	0.6	**80.6**	1.4	1.8	0.8	0.7	0.8	0.6	12.7

3.3.2 Interpretability

As noted by PlatePlate (1999), one of the chief advantages of additive models such as GAM is their interpretability. Plate also notes that by allowing high-order interactions as well as low-order interactions, one can trade off interpretability with predictive accuracy. In the case where the hyperparameters indicate that most of the variance in a function can be explained by low-order interactions, it is useful and easy to plot the corresponding low-order functions, as in Figure 3.2.

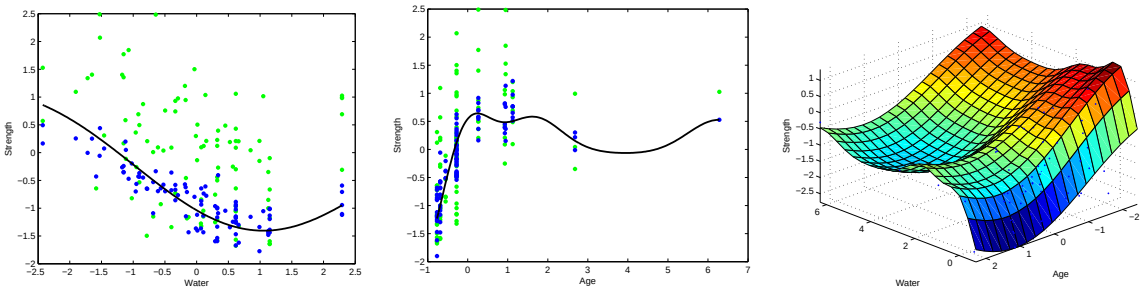

Fig. 3.2 Low-order functions on the concrete dataset. Left, Centre: By considering only first-order terms of the additive kernel, we recover a form of Generalized Additive Model, and can plot the corresponding 1-dimensional functions. Green points indicate the original data, blue points are data after the mean contribution from the other dimensions' first-order terms has been subtracted. The black line is the posterior mean of a GP with only one term in its kernel. Right: The posterior mean of a GP with only one second-order term in its kernel.

3.3.3 Efficient Evaluation of Additive Kernels

An additive kernel over D inputs with interactions up to order n has $O(2^n)$ terms. Naïvely summing over these terms quickly becomes intractable. In this section, we show how one can evaluate the sum over all terms in $O(D^2)$.

The nth order additive kernel corresponds to the nth *elementary symmetric polynomial*Macdonald (1998) Stanley (2001), which we denote e_n. For example: if $\mathbf{x}$ has 4 input dimensions ($D = 4$), and if we let $z_i = k_i(x_i, x_i')$, then

$$
\begin{aligned}
k_{add_1}(\mathbf{x}, \mathbf{x}') &= e_1(z_1, z_2, z_3, z_4) = z_1 + z_2 + z_3 + z_4 \\
k_{add_2}(\mathbf{x}, \mathbf{x}') &= e_2(z_1, z_2, z_3, z_4) = z_1 z_2 + z_1 z_3 + z_1 z_4 + z_2 z_3 + z_2 z_4 + z_3 z_4 \\
k_{add_3}(\mathbf{x}, \mathbf{x}') &= e_3(z_1, z_2, z_3, z_4) = z_1 z_2 z_3 + z_1 z_2 z_4 + z_1 z_3 z_4 + z_2 z_3 z_4 \\
k_{add_4}(\mathbf{x}, \mathbf{x}') &= e_4(z_1, z_2, z_3, z_4) = z_1 z_2 z_3 z_4
\end{aligned}
$$

The Newton-Girard formulae give an efficient recursive form for computing these polynomials. If we define s_k to be the kth power sum: $s_k(z_1, z_2, \ldots, z_D) = \sum_{i=1}^{D} z_i^k$, then

$$
k_{add_n}(\mathbf{x}, \mathbf{x}') = e_n(z_1, \ldots, z_D) = \frac{1}{n} \sum_{k=1}^{n} (-1)^{(k-1)} e_{n-k}(z_1, \ldots, z_D) s_k(z_1, \ldots, z_D) \tag{3.6}
$$

Where $e_0 \triangleq 1$. The Newton-Girard formulae have time complexity $O(D^2)$, while computing a sum over an exponential number of terms.

Conveniently, we can use the same trick to efficiently compute all of the necessary derivatives of the additive kernel with respect to the base kernels. We merely need to remove the kernel of interest from each term of the polynomials:

$$
\frac{\partial k_{add_n}}{\partial z_j} = e_{n-1}(z_1, \ldots, z_{j-1}, z_{j+1}, \ldots z_D) \tag{3.7}
$$

This trick allows us to optimize the base kernel hyperparameters with respect to the marginal likelihood.

3.3.4 Computation

The computational cost of evaluating the Gram matrix of a product kernel (such as the SE kernel) is $O(N^2 D)$, while the cost of evaluating the Gram matrix of the additive kernel is $O(N^2 DR)$, where R is the maximum degree of interaction allowed (up to D).

In higher dimensions, this can be a significant cost, even relative to the fixed $O(N^3)$ cost of inverting the Gram matrix. However, as our experiments show, typically only the first few orders of interaction are important for modeling a given function; hence if one is computationally limited, one can simply limit the maximum degree of interaction without losing much accuracy.

Additive Gaussian processes are particularly appealing in practice because their use requires only the specification of the base kernel. All other aspects of GP inference remain the same. All of the experiments in this paper were performed using the standard GPML toolbox[1]; code to perform all experiments is available at the author's website.[2]

3.4 Related Work

PlatePlate (1999) constructs a form of additive GP, but using only the first-order and Dth order terms. This model is motivated by the desire to trade off the interpretability of first-order models, with the flexibility of full-order models. Our experiments show that often, the intermediate degrees of interaction contribute most of the variance.

A related functional ANOVA GP modelKaufman and Sain (2010) decomposes the *mean* function into a weighted sum of GPs. However, the effect of a particular degree of interaction cannot be quantified by that approach. Also, computationally, the Gibbs sampling approach used in Kaufman and Sain (2010) is disadvantageous.

Christoudias et al.Christoudias et al. (2009) previously showed how mixtures of kernels can be learnt by gradient descent in the Gaussian process framework. They call this *Bayesian localized multiple kernel learning*. However, their approach learns a mixture over a small, fixed set of kernels, while our method learns a mixture over all possible products of those kernels.

3.4.1 Hierarchical Kernel Learning

BachBach (2009) uses a regularized optimization framework to learn a weighted sum over an exponential number of kernels which can be computed in polynomial time. The subsets of kernels considered by this method are restricted to be a *hull* of kernels.[3] Given

[1] Available at `http://www.gaussianprocess.org/gpml/code/`

[2] Example code available at: `http://mlg.eng.cam.ac.uk/duvenaud/`

[3] In the setting we are considering in this paper, a hull can be defined as a subset of all terms such that if term $\prod_{j \in J} k_j(\mathbf{x}, \mathbf{x}')$ is included in the subset, then so are all terms $\prod_{j \in J/i} k_j(\mathbf{x}, \mathbf{x}')$, for all $i \in J$. For details, see Bach (2009).

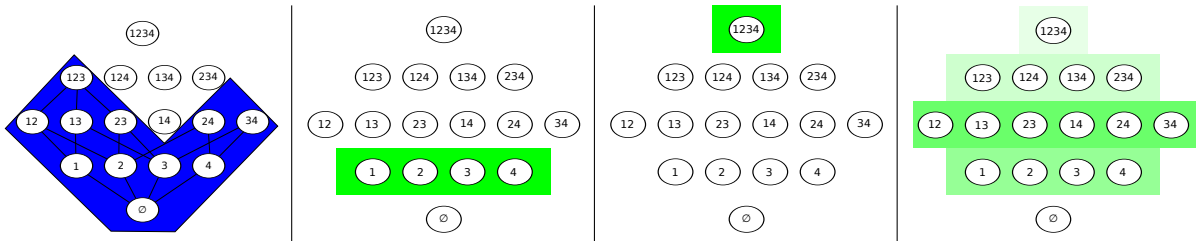

Fig. 3.3 A comparison of different models. Nodes represent different interaction terms, ranging from first-order to fourth-order interactions. Far left: HKL can select a hull of interaction terms, but must use a pre-determined weighting over those terms. Far right: the additive GP model can weight each order of interaction seperately. Neither the HKL nor the additive model dominate one another in terms of flexibility, however the GP-GAM and the SE-GP are special cases of additive GPs.

each dimension's kernel, and a pre-defined weighting over all terms, HKL performs model selection by searching over hulls of interaction terms. In Bach (2009), Bach also fixes the relative weighting between orders of interaction with a single term α, computing the sum over all orders by:

$$k_a(\mathbf{x}, \mathbf{x}') = v_D^2 \prod_{d=1}^{D} (1 + \alpha k_d(x_d, x'_d)) \tag{3.8}$$

which has computational complexity $O(D)$. However, this formulation forces the weight of all nth order terms to be weighted by α^n.

Figure 3.3 contrasts the HKL hull-selection method with the Additive GP hyperparameter-learning method. Neither method dominates the other in flexibility. The main difficulty with the approach of Bach (2009) is that hyperparameters are hard to set other than by cross-validation. In contrast, our method optimizes the hyperparameters of each dimension's base kernel, as well as the relative weighting of each order of interaction.

3.4.2 ANOVA Procedures

Vapnik Vapnik (1998) introduces the support vector ANOVA decomposition, which has the same form as our additive kernel. However, they recommend approximating the sum over all D orders with only one term "of appropriate order", presumably because of the difficulty of setting the hyperparameters of an SVM. Stitson et al.Stitson et al. (1999) performed experiments which favourably compared the support vector ANOVA

decomposition to polynomial and spline kernels. They too allowed only one order to be active, and set hyperparameters by cross-validation.

A closely related procedure from the statistics literature is smoothing-splines ANOVA (SS-ANOVA)Wahba (1990). An SS-ANOVA model is estimated as a weighted sum of splines along each dimension, plus a sum of splines over all pairs of dimensions, all triplets, etc, with each individual interaction term having a separate weighting parameter. Because the number of terms to consider grows exponentially in the order, in practice, only terms of first and second order are usually considered. Learning in SS-ANOVA is usually done via penalized-maximum likelihood with a fixed sparsity hyperparameter.

In contrast to these procedures, our method can easily include all D orders of interaction, each weighted by a separate hyperparameter. As well, we can learn kernel hyperparameters individually per input dimension, allowing automatic relevance determination to operate.

3.4.3 Non-local Interactions

By far the most popular kernels for regression and classification tasks on continuous data are the squared exponential (Gaussian) kernel, and the Matérn kernels. These kernels depend only on the scaled Euclidean distance between two points, both having the form: $k(\mathbf{x}, \mathbf{x}') = f(\sum_{d=1}^{D} (x_d - x'_d)^2 / l_d^2)$. Bengio et al.Bengio et al. (2006a) argue that models based on squared-exponential kernels are particularily susceptible to the *curse of dimensionality*. They emphasize that the locality of the kernels means that these models cannot capture non-local structure. They argue that many functions that we care about have such structure. Methods based solely on local kernels will require training examples at all combinations of relevant inputs.

Additive kernels have a much more complex structure, and allow extrapolation based on distant parts of the input space, without spreading the mass of the kernel over the whole space. For example, additive kernels of the second order allow strong non-local interactions between any points which are similar in any two input dimensions. Figure 3.4 provides a geometric comparison between squared-exponential kernels and additive kernels in 3 dimensions.

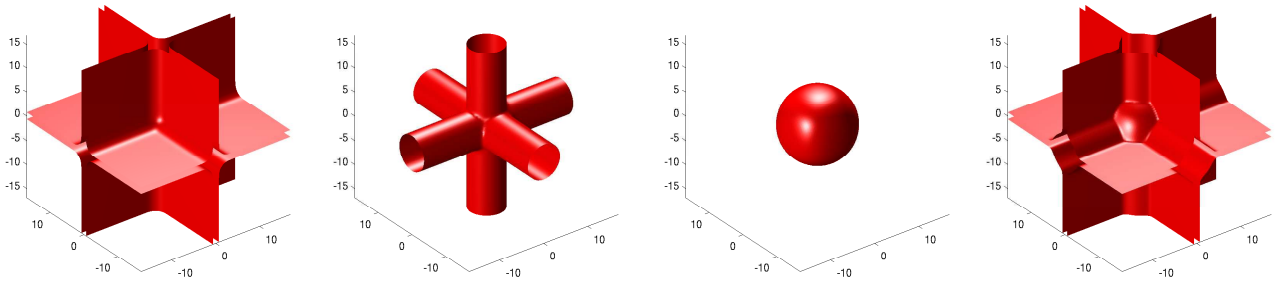

1st order interactions $k_1 + k_2 + k_3$ | 2nd order interactions $k_1k_2 + k_2k_3 + k_1k_3$ | 3rd order interactions $k_1k_2k_3$ (Squared-exp kernel) | All interactions (Additive kernel)

Fig. 3.4 Isocontours of additive kernels in 3 dimensions. The third-order kernel only considers nearby points relevant, while the lower-order kernels allow the output to depend on distant points, as long as they share one or more input value.

3.5 Experiments

3.5.1 Synthetic Data

Because additive kernels can discover non-local structure in data, they are exceptionally well-suited to problems where local interpolation fails. Figure 3.5 shows a dataset which

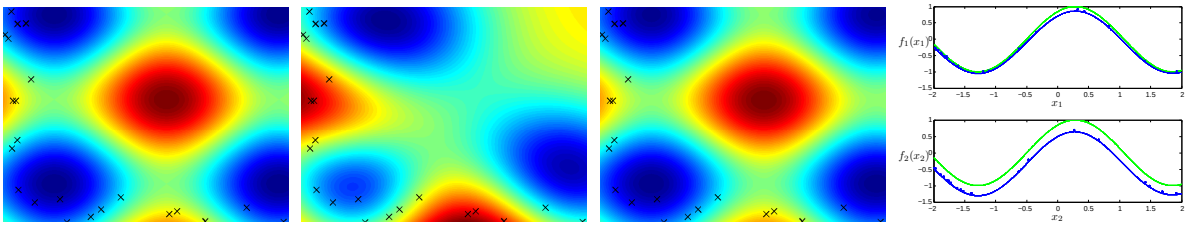

True Function & data locations | Squared-exp GP posterior mean | Additive GP posterior mean | Additive GP 1st-order functions

Fig. 3.5 Long-range inference in functions with additive structure.

demonstrates this feature of additive GPs, consisting of data drawn from a sum of two axis-aligned sine functions. The training set is restricted to a small, L-shaped area; the test set contains a peak far from the training set locations. The additive GP recovered both of the original sine functions (shown in green), and inferred correctly that most of the variance in the function comes from first-order interactions. The ability of additive GPs to discover long-range structure suggests that this model may be well-suited to deal with covariate-shift problems.

3.5.2 Experimental Setup

On a diverse collection of datasets, we compared five different models. In the results tables below, GP Additive refers to a GP using the additive kernel with squared-exp base kernels. For speed, we limited the maximum order of interaction in the additive kernels to 10. GP-GAM denotes an additive GP model with only first-order interactions. GP Squared-Exp is a GP model with a squared-exponential ARD kernel. HKL[4] was run using the all-subsets kernel, which corresponds to the same set of kernels as considered by the additive GP with a squared-exp base kernel.

For all GP models, we fit hyperparameters by the standard method of maximizing training-set marginal likelihood, using L-BFGS Nocedal (1980) for 500 iterations, allowing five random restarts. In addition to learning kernel hyperparameters, we fit a constant mean function to the data. In the classification experiments, GP inference was done using Expectation Propagation Minka (2001).

3.5.3 Results

Tables 4.2, 3.3, 3.4 and 3.5 show mean performance across 10 train-test splits. Because HKL does not specify a noise model, it could not be included in the likelihood comparisons.

Table 3.2 Regression Mean Squared Error

Method	bach	concrete	pumadyn-8nh	servo	housing
Linear Regression	1.031	0.404	0.641	0.523	0.289
GP GAM	1.259	0.149	0.598	0.281	0.161
HKL	**0.199**	0.147	0.346	0.199	0.151
GP Squared-exp	**0.045**	0.157	**0.317**	**0.126**	**0.092**
GP Additive	**0.045**	**0.089**	**0.316**	**0.110**	**0.102**

The model with best performance on each dataset is in bold, along with all other models that were not significantly different under a paired t-test. The additive model never performs significantly worse than any other model, and sometimes performs significantly better than all other models. The difference between all methods is larger in the case of regression experiments. The performance of HKL is consistent with the results in Bach (2009), performing competitively but slightly worse than SE-GP.

[4]Code for HKL available at `http://www.di.ens.fr/~fbach/hkl/`

Table 3.3 Regression Negative Log Likelihood

Method	bach	concrete	pumadyn-8nh	servo	housing
Linear Regression	2.430	1.403	1.881	1.678	1.052
GP GAM	1.708	0.467	1.195	0.800	0.457
GP Squared-exp	**−0.131**	0.398	**0.843**	0.429	**0.207**
GP Additive	**−0.131**	**0.114**	**0.841**	**0.309**	**0.194**

Table 3.4 Classification Percent Error

Method	breast	pima	sonar	ionosphere	liver	heart
Logistic Regression	7.611	24.392	26.786	16.810	45.060	**16.082**
GP GAM	**5.189**	**22.419**	**15.786**	**8.524**	**29.842**	**16.839**
HKL	**5.377**	24.261	**21.000**	9.119	**27.270**	**18.975**
GP Squared-exp	**4.734**	**23.722**	**16.357**	**6.833**	**31.237**	**20.642**
GP Additive	**5.566**	**23.076**	**15.714**	**7.976**	**30.060**	**18.496**

Table 3.5 Classification Negative Log Likelihood

Method	breast	pima	sonar	ionosphere	liver	heart
Logistic Regression	0.247	0.560	4.609	0.878	0.864	0.575
GP GAM	**0.163**	**0.461**	**0.377**	**0.312**	**0.569**	**0.393**
GP Squared-exp	**0.146**	0.478	**0.425**	**0.236**	**0.601**	0.480
GP Additive	**0.150**	**0.466**	**0.409**	**0.295**	**0.588**	**0.415**

The additive GP performed best on datasets well-explained by low orders of interaction, and approximately as well as the SE-GP model on datasets which were well explained by high orders of interaction (see table 3.1). Because the additive GP is a superset of both the GP-GAM model and the SE-GP model, instances where the additive GP performs slightly worse are presumably due to over-fitting, or due to the hyperparameter optimization becoming stuck in a local maximum. Additive GP performance can be expected to benefit from integrating out the kernel hyperparameters.

3.6 Conclusion

We present additive Gaussian processes: a simple family of models which generalizes two widely-used classes of models. Additive GPs also introduce a tractable new type of structure into the GP framework. Our experiments indicate that such additive structure is present in real datasets, allowing our model to perform better than standard GP models. In the case where no such structure exists, our model can recover arbitrarily flexible models, as well.

In addition to improving modeling efficacy, the additive GP also improves model interpretability: the order variance hyperparameters indicate which sorts of structure are present in our model.

Compared to HKL, which is the only other tractable procedure able to capture the same types of structure, our method benefits from being able to learn individual kernel hyperparameters, as well as the weightings of different orders of interaction. Our experiments show that additive GPs are a state-of-the-art regression model.

3.6.1 Bach Synthetic Dataset

In addition to standard UCI repository datasets, we generated a synthetic dataset following the same recipe as Bach (2009): From a covariance matrix drawn from a Wishart distribution with 1024 degrees of freedom, we select 8 variables. We then construct the non-linear function $f(X) = \sum_{i=1}^{4} \sum_{j=1+1}^{4} X_i X_j + \epsilon$, which sums all 2-way products of the first 4 variables, and adds Gaussian noise ϵ. This dataset is one which can be predicted well by a kernel which is a sum of two-way interactions over the first 4 variables, ignoring the extra 4 noisy copies.

This dataset was designed by Bach (2009) to demonstrate the advantages of HKL over GP-ARD.

If the dataset is large enough, HKL can construct a hull around only those subsets of cross terms that are optimal for predicting the output. GP-ARD, in contrast, can only learn to ignore the noisy copy variables, but cannot learn to ignore the higher-term interactions between the predictive variables. However, a GP with an additive kernel can learn both to ignore irrelevant variables, and to ignore certain orders of interaction. In this example, the additive GP is able to recover the relevant structure.

Table 3.6 shows the hyperparameters learnt. Note that while GP-ARD increases the lengthscale of the irrelevant variables, GP-AS reduces the signal variance.

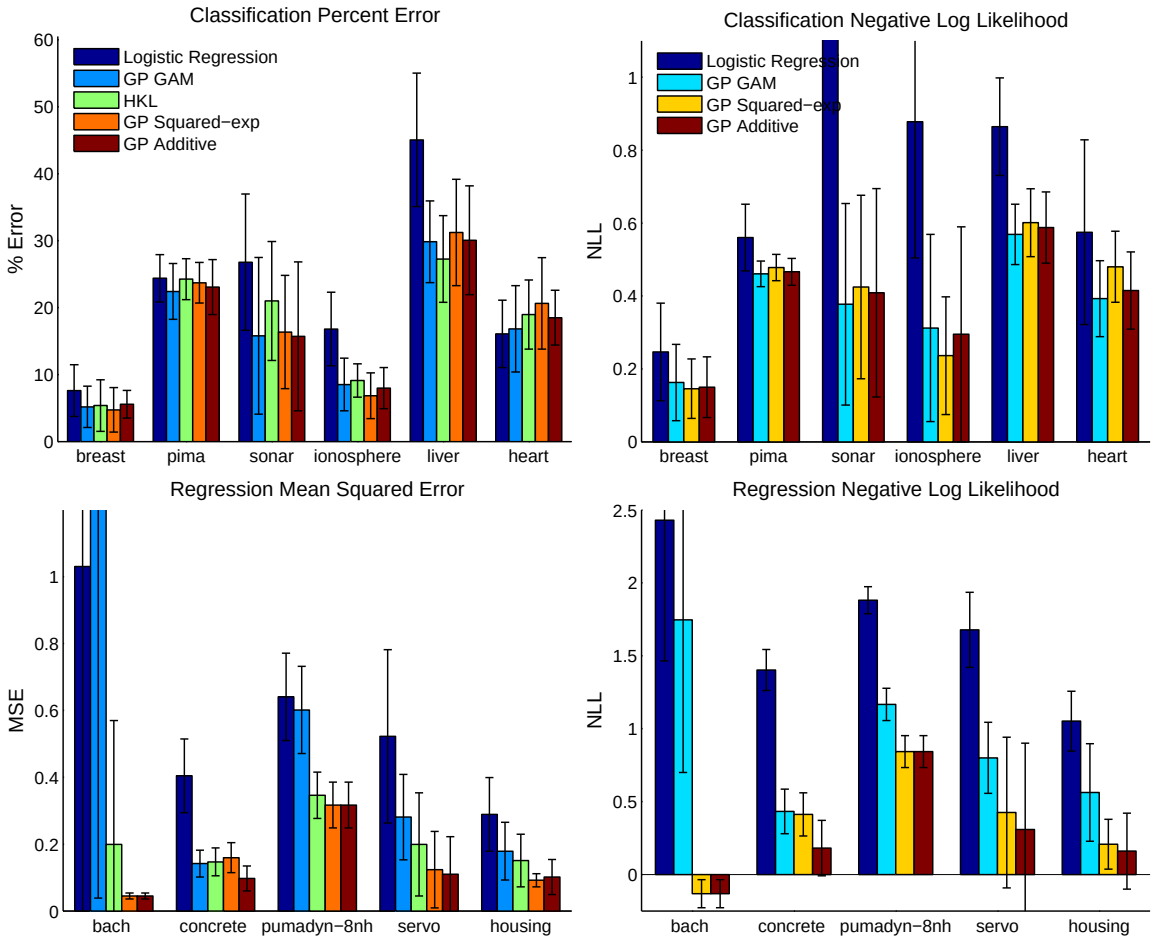
Classification Percent Error
% Error
Logistic Regression
GP GAM
HKL
GP Squared−exp
GP Additive
breast
pima
sonar
ionosphere
liver
heart
Classification Negative Log Likelihood
NLL
Logistic Regression
GP GAM
GP Squared−exp
GP Additive
Regression Mean Squared Error
MSE
bach
concrete
pumadyn−8nh
servo
housing
Regression Negative Log Likelihood
NLL

Table 3.6 Hyperparameters for bach synth c 200 dataset

Variable:	x_1	x_2	x_3	x_4	x_5	x_6	x_7	x_8
ARD Lengthscale	1.09	0.32	0.09	0.74	760.60	522.32	667.74	886.37
ADD Lengthscale	0.93	0.83	0.04	0.62	473.04	325.51	415.76	551.96
ADD Variance	15.48	21.02	0.01	60.93	0.67	0.67	0.67	0.67
Order of Interaction:	1	2	3	4	5	6	7	8
ADD Order Variance	0.0%	0.0%	0.0%	0.0%	0.0%	49.0%	0.1%	50.8%

3.6.2 Polynomial Kernels

A simple variation on the all-subsets kernel would be one which includes repeated terms, of the form

$$k_{h_n}(\mathbf{x}, \mathbf{x}') = v_n^2 \sum_{i_1,\ldots,i_n} \prod_{d=1}^{n} k_{i_d}(x_{i_d}, x'_{i_d}) = v_n^2 \prod_{d=1}^{n} \sum_{i_1,\ldots,i_n}^{n} k_{i_d}(x_{i_d}, x'_{i_d}) \tag{3.9}$$

This formulation allows repeated terms, such as x_i^2 and is equivalent to the polynomial kernelShawe-Taylor and Cristianini (2004). However, this formulation cases the length scale of each dimension to vary with the order of interaction considered.

3.6.3 Future Work

Since the non-local structure capturable by additive kernels is necessarily axis-aligned, we can naturally consider that combining the hyperparameter optimization with an initial rotation of the input space might allow us to recover non-axis aligned additivity in functions.

A Gaussian process with an additive kernel corresponds to a prior over functions which are additive. If a function $\mathbf{f} = \mathbf{a} + \mathbf{b}$ is a sum of two functions $\mathbf{a}$ and $\mathbf{b}$ drawn from a Gaussian process prior with covariances $\mathbf{K_a}$ and $\mathbf{K_b}$, then equivalently, f is drawn from a Gaussian process prior with covariance $\mathbf{K_f} = \mathbf{K_a} + \mathbf{K_b}$. The converse also holds. If $\mathbf{K_a}$ and $\mathbf{K_b}$ are positive definite, then so is $\mathbf{K_f}$.

Note that we are free to choose a different covariance function along each dimension.

[Explain how squared exp somehow puts too much mass on complicated hypotheses, or is unable to represent simple hypotheses].

[Show differences in marginal likelihoods]

[Should we try learning a convex hull of features as well?]

[To discuss: Shawe-Taylor says in Remark 9.3 that we can control the relative weights of the degree monomials by just computing $\prod(k(x, x') + R)$. If R is high then the high-degree monomials don't matter as much. Seems like we end up with a huge constant at the end, though...]

Shawe-Taylor and Cristianini (2004) define ANOVA kernels thusly: "The ANOVA kernel of degree d is like the all-subsets kernel except that it is restricted to subsets of the given cardinality d."

Chapter 4

Automatically Building Structured Covariance Functions

Joint work with James Robert Lloyd, Roger Grosse, Joshua B. Tenenbaum, Zoubin Ghahramani

Despite its importance, choosing the structural form of the kernel in nonparametric regression remains a black art. We define a space of kernel structures which are built compositionally by adding and multiplying a small number of base kernels. We present a method for searching over this space of structures which mirrors the scientific discovery process. The learned structures can often decompose functions into interpretable components and enable long-range extrapolation on time-series datasets. Our structure search method outperforms many widely used kernels and kernel combination methods on a variety of prediction tasks.

4.1 Introduction

Kernel-based nonparametric models, such as support vector machines and Gaussian processes (gps), have been one of the dominant paradigms for supervised machine learning over the last 20 years. These methods depend on defining a kernel function, $k(x, x')$, which specifies how similar or correlated outputs y and y' are expected to be at two inputs x and x'. By defining the measure of similarity between inputs, the kernel determines the pattern of inductive generalization.

Most existing techniques pose kernel learning as a (possibly high-dimensional) parameter estimation problem. Examples include learning hyperparameters (Rasmussen and Williams, 2006), linear combinations of fixed kernels **?**, and mappings from the input

space to an embedding space **?**.

However, to apply existing kernel learning algorithms, the user must specify the parametric form of the kernel, and this can require considerable expertise, as well as trial and error.

To make kernel learning more generally applicable, we reframe the kernel learning problem as one of structure discovery, and automate the choice of kernel form. In particular, we formulate a space of kernel structures defined compositionally in terms of sums and products of a small number of base kernel structures. This provides an expressive modeling language which concisely captures many widely used techniques for constructing kernels. We focus on Gaussian process regression, where the kernel specifies a covariance function, because the Bayesian framework is a convenient way to formalize structure discovery. Borrowing discrete search techniques which have proved successful in equation discovery **?** and unsupervised learning **?**, we automatically search over this space of kernel structures using marginal likelihood as the search criterion.

We found that our structure discovery algorithm is able to automatically recover known structures from synthetic data as well as plausible structures for a variety of real-world datasets. On a variety of time series datasets, the learned kernels yield decompositions of the unknown function into interpretable components that enable accurate extrapolation beyond the range of the observations. Furthermore, the automatically discovered kernels outperform a variety of widely used kernel classes and kernel combination methods on supervised prediction tasks.

While we focus on Gaussian process regression, we believe our kernel search method can be extended to other supervised learning frameworks such as classification or ordinal regression, or to other kinds of kernel architectures such as kernel SVMs. We hope that the algorithm developed in this paper will help replace the current and often opaque art of kernel engineering with a more transparent science of automated kernel construction.

4.2 Expressing structure through kernels

Gaussian process models use a kernel to define the covariance between any two function values: $\mathrm{Cov}(y, y') = k(x, x')$. The kernel specifies which structures are likely under the gp prior, which in turn determines the generalization properties of the model. In this section, we review the ways in which kernel families[1] can be composed to express diverse

priors over functions.

There has been significant work on constructing gp kernels and analyzing their properties, summarized in Chapter 4 of Rasmussen and Williams (2006). Commonly used kernels families include the squared exponential (SE), periodic (Per), linear (Lin), and rational quadratic (RQ) (see Figure 4.1 and the appendix).

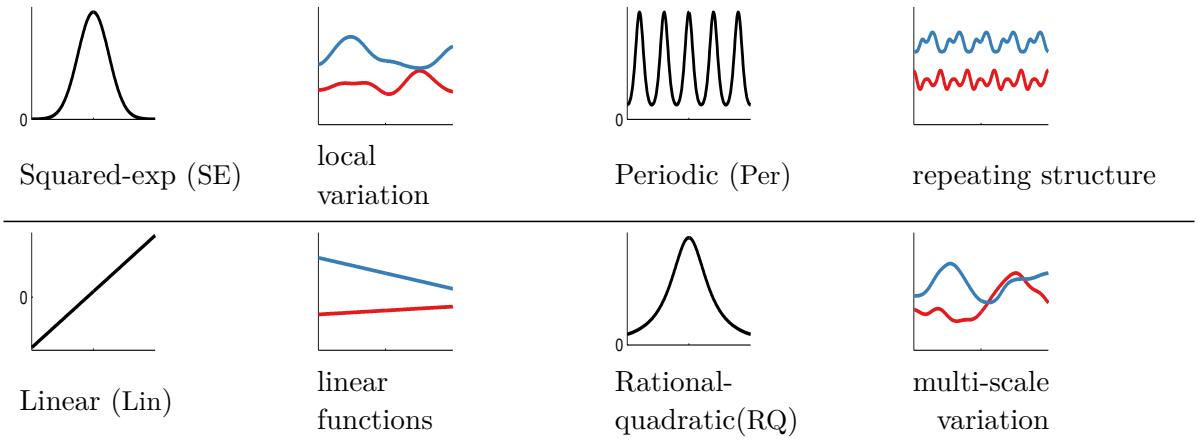

Fig. 4.1 Left and third columns: base kernels $k(\cdot, 0)$. Second and fourth columns: draws from a GP with each repective kernel. The x-axis has the same range on all plots.

Composing Kernels Positive semidefinite kernels (i.e. those which define valid covariance functions) are closed under addition and multiplication. This allows one to create richly structured and interpretable kernels from well understood base components.

All of the base kernels we use are one-dimensional; kernels over multidimensional inputs are constructed by adding and multiplying kernels over individual dimensions. These dimensions are represented using subscripts, e.g. SE_2 represents an SE kernel over the second dimension of x.

Summation By summing kernels, we can model the data as a superposition of independent functions, possibly representing different structures. Suppose functions f_1, f_2 are draw from independent gp priors, $f_1 \sim \mathcal{GP}(\mu_1, k_1)$, $f_2 \sim \mathcal{GP}(\mu_2, k_2)$. Then $f := f_1 + f_2 \sim \mathcal{GP}(\mu$

In time series models, sums of kernels can express superposition of different processes, possibly operating at different scales. In multiple dimensions, summing kernels gives additive structure over different dimensions, similar to generalized additive models (Hastie

[1]When unclear from context, we use 'kernel family' to refer to the parametric forms of the functions given in the appendix. A kernel is a kernel family with all of the parameters specified.

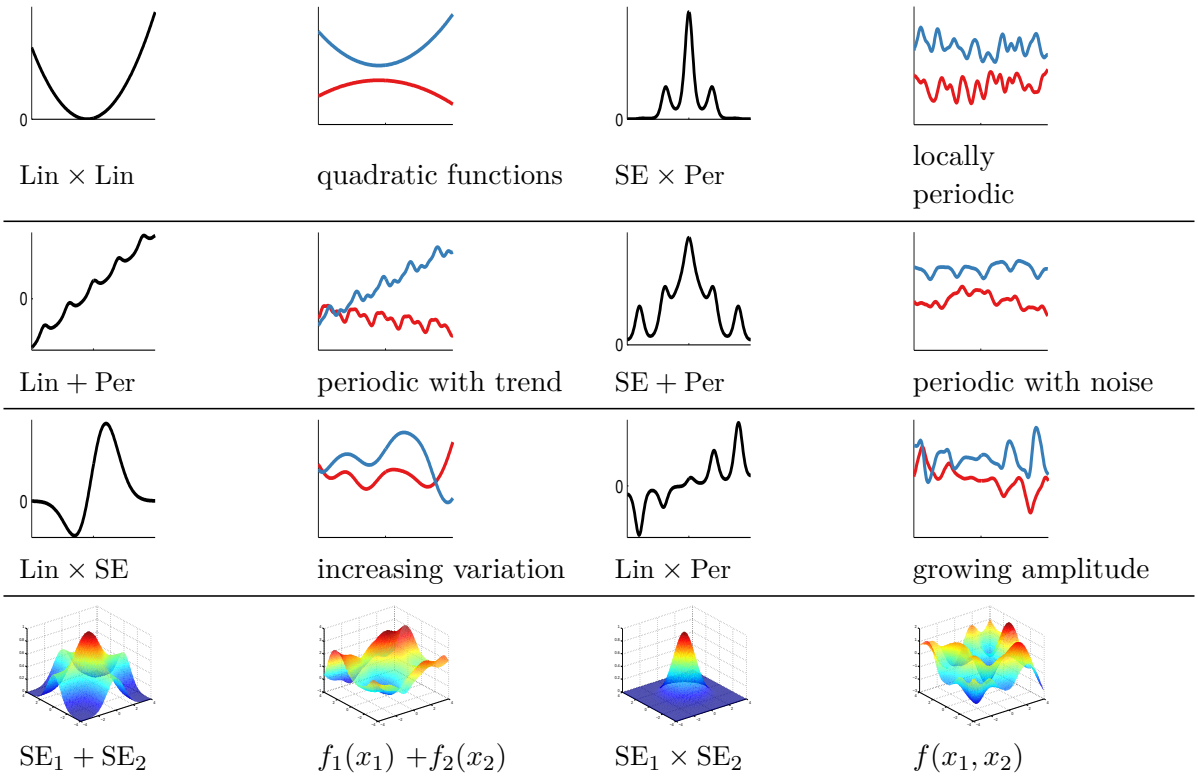

Fig. 4.2 Examples of structures expressible by composite kernels. Left column and third columns: composite kernels $k(\cdot, 0)$. Plots have same meaning as in Figure 4.1.

and Tibshirani, 1990). These two kinds of structure are demonstrated in rows 2 and 4 of figure 4.2, respectively.

Multiplication Multiplying kernels allows us to account for interactions between different input dimensions or different notions of similarity. For instance, in multidimensional data, the multiplicative kernel $\mathrm{SE}_1 \times \mathrm{SE}_3$ represents a smoothly varying function of dimensions 1 and 3 which is not constrained to be additive. In univariate data, multiplying a kernel by SE gives a way of converting global structure to local structure. For example, Per corresponds to globally periodic structure, whereas Per × SE corresponds to locally periodic structure, as shown in row 1 of figure 4.2.

Many architectures for learning complex functions, such as convolutional networks **?** and sum-product networks **?**, include units which compute AND-like and OR-like operations. Composite kernels can be viewed in this way too. A sum of kernels can be understood as an OR-like operation: two points are considered similar if either kernel has a high value. Similarly, multiplying kernels is an AND-like operation, since two points are considered similar only if both kernels have high values. Since we are applying these

operations to the similarity functions rather than the regression functions themselves, compositions of even a few base kernels are able to capture complex relationships in data which do not have a simple parametric form.

Example expressions In addition to the examples given in Figure 4.2, many common motifs of supervised learning can be captured using sums and products of one-dimensional base kernels:

Bayesian linear regression	Lin
Bayesian polynomial regression	$\text{Lin} \times \text{Lin} \times \ldots$
Generalized Fourier decomposition	$\text{Per} + \text{Per} + \ldots$
Generalized additive models	$\sum_{d=1}^{D} \text{SE}_d$
Automatic relevance determination	$\prod_{d=1}^{D} \text{SE}_d$
Linear trend with local deviations	$\text{Lin} + \text{SE}$
Linearly growing amplitude	$\text{Lin} \times \text{SE}$

We use the term 'generalized Fourier decomposition' to express that the periodic functions expressible by a gp with a periodic kernel are not limited to sinusoids.

4.3 Searching over structures

As discussed above, we can construct a wide variety of kernel structures compositionally by adding and multiplying a small number of base kernels. In particular, we consider the four base kernel families discussed in Section 4.2: SE, Per, Lin, and RQ. Any algebraic expression combining these kernels using the operations $+$ and $\times$ defines a kernel family, whose parameters are the concatenation of the parameters for the base kernel families.

Our search procedure begins by proposing all base kernel families applied to all input dimensions. We allow the following search operators over our set of expressions:

(1) Any subexpression $\mathcal{S}$ can be replaced with $\mathcal{S}+\mathcal{B}$, where $\mathcal{B}$ is any base kernel family.

(2) Any subexpression $\mathcal{S}$ can be replaced with $\mathcal{S}\times\mathcal{B}$, where $\mathcal{B}$ is any base kernel family.

(3) Any base kernel $\mathcal{B}$ may be replaced with any other base kernel family $\mathcal{B}'$.

These operators can generate all possible algebraic expressions. To see this, observe that if we restricted the $+$ and $\times$ rules only to apply to base kernel families, we would obtain a context-free grammar (CFG) which generates the set of algebraic expressions.

However, the more general versions of these rules allow more flexibility in the search procedure, which is useful because the CFG derivation may not be the most straightforward way to arrive at a kernel family.

Our algorithm searches over this space using a greedy search: at each stage, we choose the highest scoring kernel and expand it by applying all possible operators.

Our search operators are motivated by strategies researchers often use to construct kernels. In particular,

- One can look for structure, e.g. periodicity, in the residuals of a model, and then extend the model to capture that structure. This corresponds to applying rule (1).

- One can start with structure, e.g. linearity, which is assumed to hold globally, but find that it only holds locally. This corresponds to applying rule (2) to obtain the structure shown in rows 1 and 3 of figure 4.2.

- One can add features incrementally, analogous to algorithms like boosting, backfitting, or forward selection. This corresponds to applying rules (1) or (2) to dimensions not yet included in the model.

Scoring kernel families Choosing kernel structures requires a criterion for evaluating structures. We choose marginal likelihood as our criterion, since it balances the fit and complexity of a model (**?**). Conditioned on kernel parameters, the marginal likelihood of a gp can be computed analytically. However, to evaluate a kernel family we must integrate over kernel parameters. We approximate this intractable integral with the Bayesian information criterion (**?**) after first optimizing to find the maximum-likelihood kernel parameters.

Unfortunately, optimizing over parameters is not a convex optimization problem, and the space can have many local optima. For example, in data with periodic structure, integer multiples of the true period (i.e. harmonics) are often local optima. To alleviate this difficulty, we take advantage of our search procedure to provide reasonable initializations: all of the parameters which were part of the previous kernel are initialized to their previous values. All parameters are then optimized using conjugate gradients, randomly restarting the newly introduced parameters. This procedure is not guaranteed to find the global optimum, but it implements the commonly used heuristic of iteratively modeling residuals.

4.4 Related Work

Nonparametric regression in high dimensions Nonparametric regression methods such as splines, locally weighted regression, and gp regression are popular because they are capable of learning arbitrary smooth functions of the data. Unfortunately, they suffer from the curse of dimensionality: it is very difficult for the basic versions of these methods to generalize well in more than a few dimensions. Applying nonparametric methods in high-dimensional spaces can require imposing additional structure on the model.

One such structure is additivity. Generalized additive models (GAM) assume the regression function is a transformed sum of functions defined on the individual dimensions: $\mathbb{E}[f(\mathbf{x})] = g^{-1}(\sum_{d=1}^{D} f_d(x_d))$. These models have a limited compositional form, but one which is interpretable and often generalizes well. In our grammar, we can capture analogous structure through sums of base kernels along different dimensions.

It is possible to add more flexibility to additive models by considering higher-order interactions between different dimensions. Additive Gaussian processes Duvenaud et al. (2011) are a gp model whose kernel implicitly sums over all possible products of one-dimensional base kernels. Plate (1999) constructs a gp with a composite kernel, summing an SE kernel along each dimension, with an SE-ARD kernel (i.e. a product of SE over all dimensions). Both of these models can be expressed in our grammar.

A closely related procedure is smoothing-splines ANOVA Wahba (1990); **?**. This model is a linear combinations of splines along each dimension, all pairs of dimensions, and possibly higher-order combinations. Because the number of terms to consider grows exponentially in the order, in practice, only terms of first and second order are usually considered.

Semiparametric regression (e.g. **?**) attempts to combine interpretability with flexibility by building a composite model out of an interpretable, parametric part (such as linear regression) and a 'catch-all' nonparametric part (such as a gp with an SE kernel). In our approach, this can be represented as a sum of SE and Lin.

Kernel learning There is a large body of work attempting to construct a rich kernel through a weighted sum of base kernels (e.g. Christoudias et al., 2009; **?**). While these approaches find the optimal solution in polynomial time, speed comes at a cost: the component kernels, as well as their hyperparameters, must be specified in advance.

Another approach to kernel learning is to learn an embedding of the data points. **?** learns an embedding of the data into a low-dimensional space, and constructs a fixed

kernel structure over that space. This model is typically used in unsupervised tasks and requires an expensive integration or optimisation over potential embeddings when generalizing to test points. **?** use a deep neural network to learn an embedding; this is a flexible approach to kernel learning but relies upon finding structure in the input density, p(x). Instead we focus on domains where most of the interesting structure is in f(x).

? derive kernels of the form SE $\times \cos(x - x')$, forming a basis for stationary kernels. These kernels share similarities with SE $\times$ Per but can express negative prior correlation, and could usefully be included in our grammar.

? and **?** learn composite kernels for support vector machines and relevance vector machines, using genetic search algorithms. Our work employs a Bayesian search criterion, and goes beyond this prior work by demonstrating the interpretability of the structure implied by composite kernels, and how such structure allows for extrapolation.

Structure discovery There have been several attempts to uncover the structural form of a dataset by searching over a grammar of structures. For example, **?**, **?** and **?** attempt to learn parametric forms of equations to describe time series, or relations between quantities. Because we learn expressions describing the covariance structure rather than the functions themselves, we are able to capture structure which does not have a simple parametric form.

? learned the structural form of a graph used to model human similarity judgments. Examples of graphs included planes, trees, and cylinders. Some of their discrete graph structures have continous analogues in our own space; e.g. $\mathrm{SE}_1 \times \mathrm{SE}_2$ and $\mathrm{SE}_1 \times \mathrm{Per}_2$ can be seen as mapping the data to a plane and a cylinder, respectively.

? performed a greedy search over a compositional model class for unsupervised learning, using a grammar and a search procedure which parallel our own. This model class contained a large number of existing unsupervised models as special cases and was able to discover such structure automatically from data. Our work is tackling a similar problem, but in a supervised setting.

4.5 Structure discovery in time series

To investigate our method's ability to discover structure, we ran the kernel search on several time-series.

As discussed in section 2, a gp whose kernel is a sum of kernels can be viewed as a sum

of functions drawn from component gps. This provides another method of visualizing the learned structures. In particular, all kernels in our search space can be equivalently written as sums of products of base kernels by applying distributivity. For example,

$$\mathrm{SE} \times (\mathrm{RQ} + \mathrm{Lin}) = \mathrm{SE} \times \mathrm{RQ} + \mathrm{SE} \times \mathrm{Lin}.$$

We visualize the decompositions into sums of components using the formulae given in the appendix. The search was run to depth 10, using the base kernels from Section 4.2.

Mauna Loa atmospheric CO_2 Using our method, we analyzed records of carbon dioxide levels recorded at the Mauna Loa observatory. Since this dataset was analyzed in detail by Rasmussen and Williams (2006), we can compare the kernel chosen by our method to a kernel constructed by human experts.

Figure 4.3 shows the posterior mean and variance on this dataset as the search depth increases. While the data can be smoothly interpolated by a single base kernel model, the extrapolations improve dramatically as the increased search depth allows more structure to be included.

Figure 4.4 shows the final model chosen by our method, together with its decomposition into additive components. The final model exhibits both plausible extrapolation and interpretable components: a long-term trend, annual periodicity and medium-term deviations; the same components chosen by Rasmussen and Williams (2006). We also plot the residuals, observing that there is little obvious structure left in the data.

Airline passenger data Figure 4.6 shows the decomposition produced by applying our method to monthly totals of international airline passengers (**?**). We observe similar components to the previous dataset: a long term trend, annual periodicity and medium-term deviations. In addition, the composite kernel captures the near-linearity of the long-term trend, and the linearly growing amplitude of the annual oscillations.

Solar irradiance Data Finally, we analyzed annual solar irradiation data from 1610 to 2011 (**?**). The posterior and residuals of the learned kernel are shown in figure 4.5. None of the models in our search space are capable of parsimoniously representing the lack of variation from 1645 to 1715. Despite this, our approach fails gracefully: the learned kernel still captures the periodic structure, and the quickly growing posterior variance demonstrates that the model is uncertain about long term structure.

4.6 Validation on synthetic data

Table 4.1 Kernels chosen by our method on synthetic data generated using known kernel structures. D denotes the dimension of the functions being modeled. SNR indicates the signal-to-noise ratio. Dashes - indicate no structure.

True Kernel	D	SNR = 10	SNR = 1	SNR = 0.
$\mathrm{SE} + \mathrm{RQ}$	1	SE	$\mathrm{SE} \times \mathrm{Per}$	SE
$\mathrm{Lin} \times \mathrm{Per}$	1	$\mathrm{Lin} \times \mathrm{Per}$	$\mathrm{Lin} \times \mathrm{Per}$	SE
$\mathrm{SE}_1 + \mathrm{RQ}_2$	2	$\mathrm{SE}_1 + \mathrm{SE}_2$	$\mathrm{Lin}_1 + \mathrm{SE}_2$	Lin
$\mathrm{SE}_1 + \mathrm{SE}_2 \times \mathrm{Per}_1 + \mathrm{SE}_3$	3	$\mathrm{SE}_1 + \mathrm{SE}_2 \times \mathrm{Per}_1 + \mathrm{SE}_3$	$\mathrm{SE}_2 \times \mathrm{Per}_1 + \mathrm{SE}_3$	-
$\mathrm{SE}_1 \times \mathrm{SE}_2$	4	$\mathrm{SE}_1 \times \mathrm{SE}_2$	$\mathrm{Lin}_1 \times \mathrm{SE}_2$	Lin
$\mathrm{SE}_1 \times \mathrm{SE}_2 + \mathrm{SE}_2 \times \mathrm{SE}_3$	4	$\mathrm{SE}_1 \times \mathrm{SE}_2 + \mathrm{SE}_2 \times \mathrm{SE}_3$	$\mathrm{SE}_1 + \mathrm{SE}_2 \times \mathrm{SE}_3$	SE
$(\mathrm{SE}_1 + \mathrm{SE}_2) \times (\mathrm{SE}_3 + \mathrm{SE}_4)$	4	$(\mathrm{SE}_1 + \mathrm{SE}_2) \times (\mathrm{SE}_3 \times \mathrm{Lin}_3 \times \mathrm{Lin}_1 + \mathrm{SE}_4)$	$(\mathrm{SE}_1 + \mathrm{SE}_2) \times \mathrm{SE}_3 \times \mathrm{SE}_4$	-

We validated our method's ability to recover known structure on a set of synthetic datasets. For several composite kernel expressions, we constructed synthetic data by first sampling 300 points uniformly at random, then sampling function values at those points from a gp prior. We then added i.i.d. Gaussian noise to the functions, at various signal-to-noise ratios (SNR).

Table 4.1 lists the true kernels we used to generate the data. Subscripts indicate which dimension each kernel was applied to. Subsequent columns show the dimensionality D of the input space, and the kernels chosen by our search for different SNRs. Dashes - indicate that no kernel had a higher marginal likelihood than modeling the data as i.i.d. Gaussian noise.

For the highest SNR, the method finds all relevant structure in all but one test. The reported additional linear structure is explainable by the fact that functions sampled from SE kernels with long length scales occasionally have near-linear trends. As the noise increases, our method generally backs off to simpler structures.

4.7 Quantitative evaluation

In addition to the qualitative evaluation in section 4.5, we investigated quantitatively how our method performs on both extrapolation and interpolation tasks.

Table 4.2 Comparison of multidimensional regression performance. Bold results are not significantly different from the best-performing method in each experiment, in a paired t-test with a p-value of 5%.

	Mean Squared Error (MSE)					Negative Log-Likelihood				
Method	bach	concrete	puma	servo	housing	bach	concrete	puma	servo	housing
Linear Regression	1.031	0.404	0.641	0.523	0.289	2.430	1.403	1.881	1.678	1.052
GAM	1.259	0.149	0.598	0.281	0.161	1.708	0.467	1.195	0.800	0.457
HKL	**0.199**	0.147	0.346	0.199	0.151	-	-	-	-	-
gp SE-ARD	**0.045**	0.157	0.317	0.126	**0.092**	**−0.131**	0.398	0.843	0.429	0.207
gp Additive	**0.045**	**0.089**	**0.316**	**0.110**	0.102	**−0.131**	**0.114**	**0.841**	**0.309**	0.194
Structure Search	**0.044**	**0.087**	**0.315**	**0.102**	**0.082**	**−0.141**	**0.065**	**0.840**	**0.265**	**0.059**

4.7.1 Extrapolation

We compared the extrapolation capabilities of our model against standard baselines[2]. Dividing the airline dataset into contiguous training and test sets, we computed the predictive mean-squared-error (MSE) of each method. We varied the size of the training set from the first 10% to the first 90% of the data.

Figure 4.7 shows the learning curves of linear regression, a variety of fixed kernel family gp models, and our method. gp models with only SE and Per kernels did not capture the long-term trends, since the best parameter values in terms of gp marginal likelihood only capture short term structure. Linear regression approximately captured the long-term trend, but quickly plateaued in predictive performance. The more richly structured gp models (SE + Per and SE × Per) eventually captured more structure and performed better, but the full structures discovered by our search outperformed the other approaches in terms of predictive performance for all data amounts.

4.7.2 High-dimensional prediction

To evaluate the predictive accuracy of our method in a high-dimensional setting, we extended the comparison of Duvenaud et al. (2011) to include our method. We performed 10 fold cross validation on 5 datasets [3] comparing 5 methods in terms of MSE and predictive likelihood. Our structure search was run up to depth 10, using the SE and RQ base kernel families.

[2]In one dimension, the predictive means of all baseline methods in table 4.2 are identical to that of a gp with an SE kernel.

[3]The data sets had dimensionalities ranging from 4 to 13, and the number of data points ranged from 150 to 450.

The comparison included three methods with fixed kernel families: Additive gps, Generalized Additive Models (GAM), and a gp with a standard SE kernel using Automatic Relevance Determination (gp SE-ARD). Also included was the related kernel-search method of Hierarchical Kernel Learning (HKL).

Results are presented in table 4.2. Our method outperformed the next-best method in each test, although not substantially.

All gp hyperparameter tuning was performed by automated calls to the GPML toolbox[4]; Python code to perform all experiments is available on github[5].

4.8 Discussion

> "It would be very nice to have a formal apparatus that gives us some 'optimal' way of recognizing unusual phenomena and inventing new classes of hypotheses that are most likely to contain the true one; but this remains an art for the creative human mind."
>
> ?

Towards the goal of automating the choice of kernel family, we introduced a space of composite kernels defined compositionally as sums and products of a small number of base kernels. The set of models included in this space includes many standard regression models. We proposed a search procedure for this space of kernels which parallels the process of scientific discovery.

We found that the learned structures are often capable of accurate extrapolation in complex time-series datasets, and are competitive with widely used kernel classes and kernel combination methods on a variety of prediction tasks. The learned kernels often yield decompositions of a signal into diverse and interpretable components, enabling model-checking by humans. We believe that a data-driven approach to choosing kernel structures automatically can help make nonparametric regression and classification methods accessible to non-experts.

[4] Available at www.gaussianprocess.org/gpml/code/
[5] github.com/jamesrobertlloyd/gp-structure-search

Appendix

Kernel definitions For scalar-valued inputs, the squared exponential (SE), periodic (Per), linear (Lin), and rational quadratic (RQ) kernels are defined as follows:

$$\begin{aligned} k_{\mathrm{SE}}(x, x') &= \sigma^2 \exp\left(-\tfrac{(x-x')^2}{2\ell^2}\right) \\ k_{\mathrm{Per}}(x, x') &= \sigma^2 \exp\left(-\tfrac{2\sin^2(\pi(x-x')/p)}{\ell^2}\right) \\ k_{\mathrm{Lin}}(x, x') &= \sigma_b^2 + \sigma_v^2(x-\ell)(x'-\ell) \\ k_{\mathrm{RQ}}(x, x') &= \sigma^2 \left(1 + \tfrac{(x-x')^2}{2\alpha\ell^2}\right)^{-\alpha} \end{aligned}$$

Posterior decomposition We can analytically decompose a gp posterior distribution over additive components using the following identity: The conditional distribution of a Gaussian vector $\mathbf{f}_1$ conditioned on its sum with another Gaussian vector $\mathbf{f} = \mathbf{f}_1 + \mathbf{f}_2$ where $\mathbf{f}_1 \sim \mathcal{N}(\mu_1, \mathbf{K}_1)$ and $\mathbf{f}_2 \sim \mathcal{N}(\mu_2, \mathbf{K}_2)$ is given by

$$\begin{aligned} \mathbf{f}_1 | \mathbf{f} \sim \mathcal{N}\Big(&\mu_1 + {\mathbf{K}_1}^{\mathsf{T}}(\mathbf{K}_1 + \mathbf{K}_2)^{-1}\left(\mathbf{f} - \mu_1 - \mu_2\right), \\ &\mathbf{K}_1 - {\mathbf{K}_1}^{\mathsf{T}}(\mathbf{K}_1 + \mathbf{K}_2)^{-1}\mathbf{K}_1\Big). \end{aligned}$$

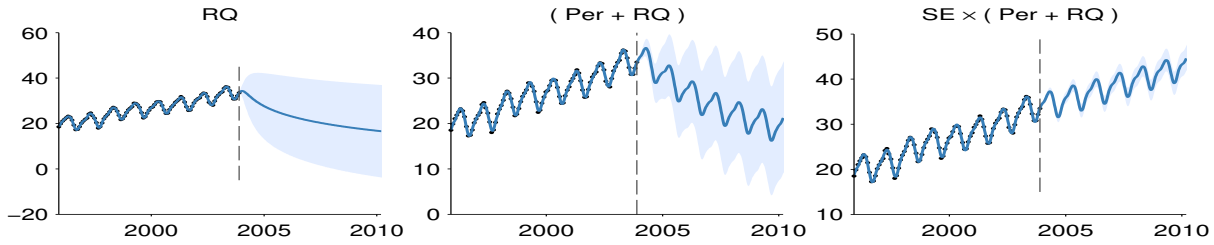

Fig. 4.3 Posterior mean and variance for different depths of kernel search. The dashed line marks the extent of the dataset. In the first column, the function is only modeled as a locally smooth function, and the extrapolation is poor. Next, a periodic component is added, and the extrapolation improves. At depth 3, the kernel can capture most of the relevant structure, and is able to extrapolate reasonably.

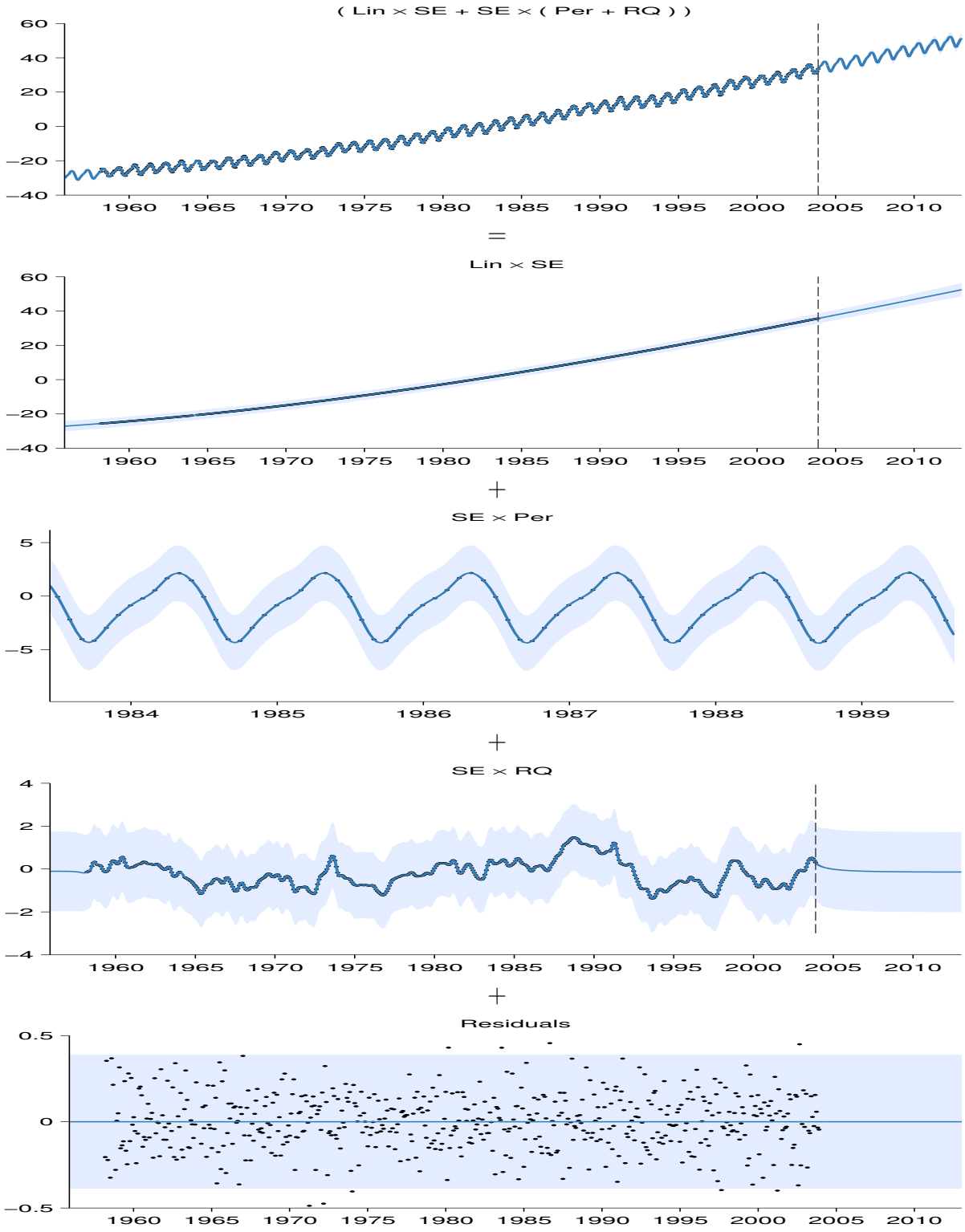

Fig. 4.4 First row: The posterior on the Mauna Loa dataset, after a search of depth 10. Subsequent rows show the automatic decomposition of the time series. The decompositions shows long-term, yearly periodic, medium-term anomaly components, and residuals, respectively. In the third row, the scale has been changed in order to clearly show the yearly periodic structure.

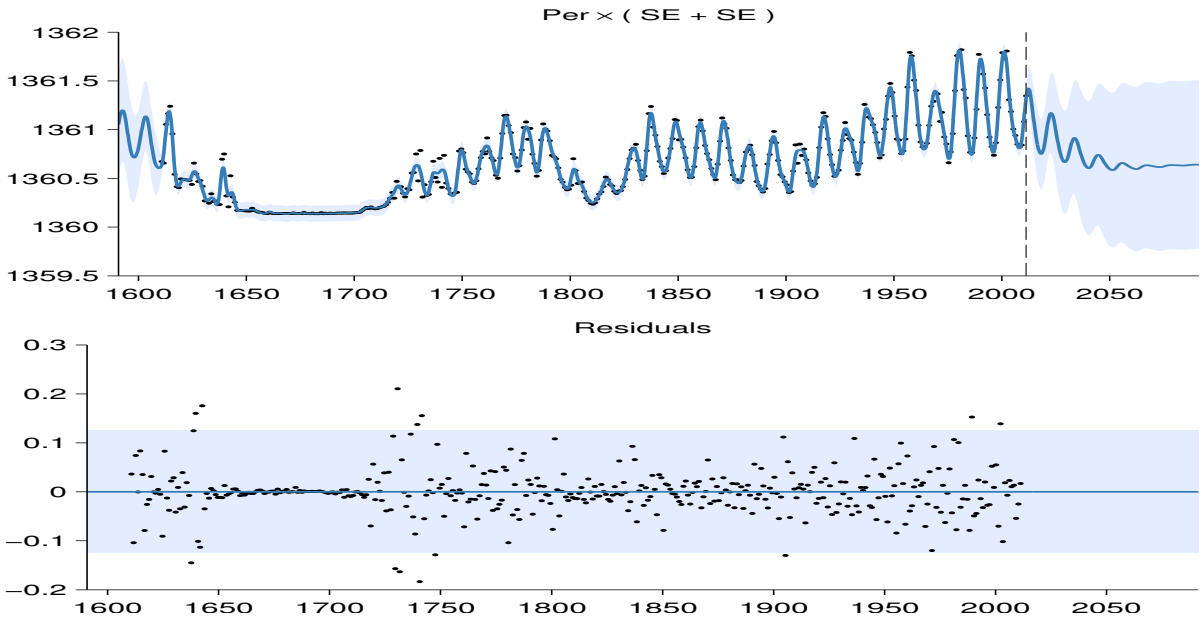

Fig. 4.5 Full posterior and residuals on the solar irradiance dataset.

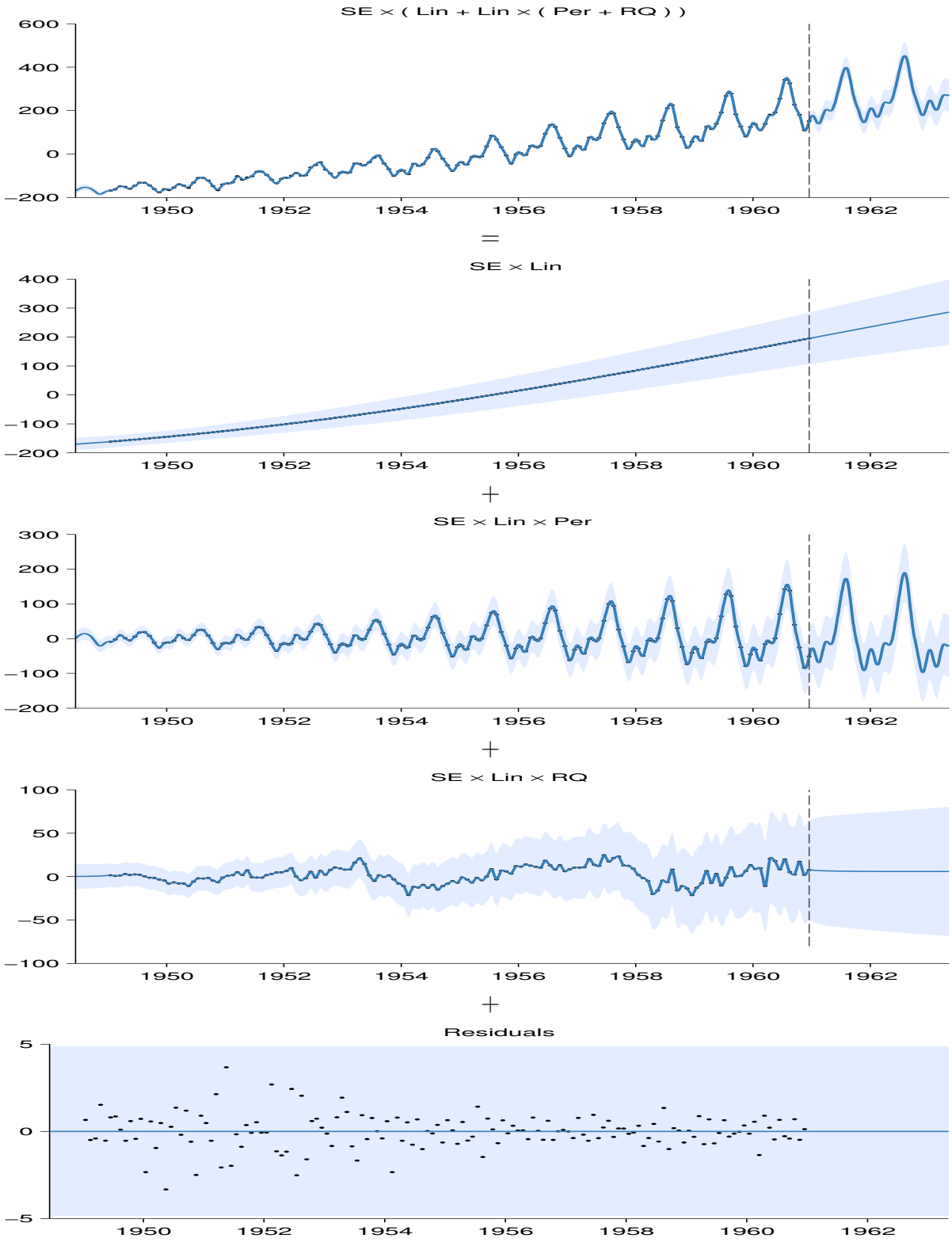

Fig. 4.6 First row: The airline dataset and posterior after a search of depth 10. Subsequent rows: Additive decomposition of posterior into long-term smooth trend, yearly variation, and short-term deviations. Due to the linear kernel, the marginal variance grows over time, making this a heteroskedastic model.

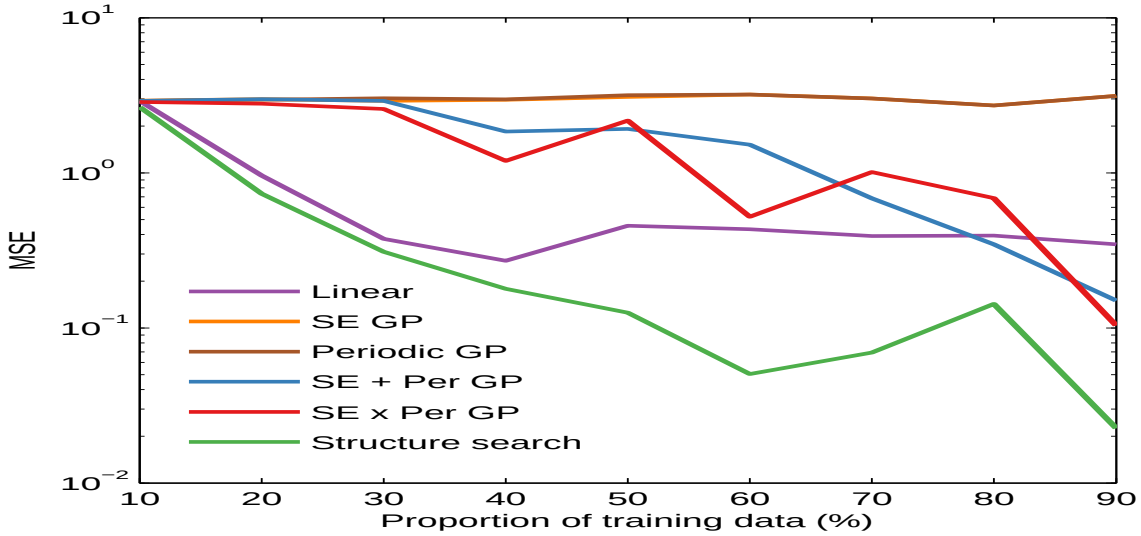

Fig. 4.7 Extrapolation performance on the airline dataset. We plot test-set MSE as a function of the fraction of the dataset used for training.

Appendix A

Bayesian Estimation of Integrals

A.1 Nonparametric Inference via Bayesian Quadrature

We extend the approximate integration method of Bayesian Quadrature to infinite structured domains, introducing a new inference method for nonparametric models.This method admits more flexible sampling schemes than Markov chains, for example active learning, and provides natural convergence diagnostics. We give conditions necessary for consistency, and show how to construct kernels between structures which take advantage of symmetries in the likelihood function. We demonstrate our inference method on both the Dirichlet process mixture model and the Indian buffet process.

A.2 Introduction

The central problem of probabilistic inference is to compute integrals over probability distributions of the form

$$Z_{f,p} = \int f(\theta)p(\theta)d\theta \tag{A.1}$$

Examples include computing marginal distributions, making predictions while marginalizing over parameters, or computing the Bayes risk in a decision problem. Machine learning has produced a rich set of methods for computing these integrals, such as Expectation Propagation[cite], Variational Bayes[cite], and many variations of Markov chain Monte Carlo (mcmc) [cite Iain Murray].

In non-parametric models, estimating (**??**) is especially challending, as the domain of integration in is infinite-dimensional. A variety of mcmc methods have been developed to

tackle this problem. However, mcmc has known weaknesses, such as difficulty diagnosing convergence, the requirement of a burn-in period, and difficulty obtaining samples from a given subset of possible θ.

Bayesian quadrature (bq) **?**, also known as Bayesian Monte Carlo **?**, is a model-based method of approximate integration. bq infers a posterior distribution over f conditioned on a set of samples $f(\theta_s)$, and gives a posterior distribution on $Z_{f,p}$. bq remains a relatively unexplored integration method, and has so far only been used in low-dimensional, continuous spaces **?**.

Summary of contributions In this paper, we extend the bq method to infinite, structured domains, introducing a new family of inference methods for non-parametric models. We give conditions necessary for consistency. We introduce kernels for inference problems using the Indian Buffet process and Dirichlet Proces mixture model which encode the many symmetries of the likelihood functions.

We then demonstrate the advantages of model-based inference on synthetic datasets, such as uncertainty estimates, flexibility in sampling methods, and post-hoc sensitivity analysis of prior and likelihood parameters. We then discuss limitations of the framework as it stands.

A.3 Bayesian Quadrature

In contrast to mcmc, a procedure which computes (**??**) in the limit of infinite samples, Bayesian quadrature is a *model-based* integration method. This means that bq puts a prior distribution on f, then conditions on some observations $f(\theta_s)$ at some query points θ_s. The posterior distribution over f then implies a distribution over $Z_{f,p}$, which can be obtained by integrating over all possible f. See Figure **??** for an illustration of Bayesian Quadrature.

It may seem circular to introduce an integral over an uncountable number of functions in order to solve what was originally an integral over a single function. However, the gpposterior has a simple form which makes integration possible in closed form in many cases. If f is assigned a Gaussian process prior with kernel function k and mean 0, then after conditioning on function evaluations $\mathbf{y} = f(\theta_1) \dots f(\theta_N)$, we obtain:

$$p(\mathbf{f}(\theta_\star)|\mathbf{y}) = \mathcal{N}\Big(\mathbf{f}(\theta_\star)|\bar{\mathbf{f}}(\theta_\star), \mathrm{cov}(\theta_\star, \theta'_\star)\Big) \tag{A.2}$$

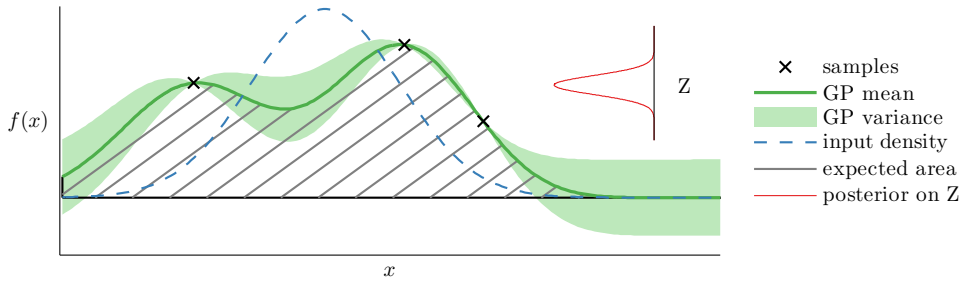

Fig. A.1 An illustration of Bayesian Quadrature. The function $f(x)$ is sampled at a set of input locations. This induces a Gaussian process posterior distribution on f, which is integrated in closed form against the target density, $p(\mathbf{x})$. Since the amount of volume under f is uncertain, this gives rise to a (Gaussian) posterior distribution over $Z_{f,p}$.

where

$$\bar{\mathbf{f}}(\mathbf{x}_\star) = k(\theta_\star, \theta_s)K^{-1}\mathbf{y} \tag{A.3}$$

$$\mathrm{cov}(\mathbf{x}_\star, \mathbf{x}'_\star) = k(\theta_\star, \theta_\star) - k(\theta_\star, \theta_s)\mathbf{K}^{-1}k(\theta_s, \theta_\star) \tag{A.4}$$

and $\mathbf{K}_{mn} = k(\theta_m, \theta_n)$. Conveniently, the gp posterior implies a closed form for the expectation and variance of (**??**):

$$\mathbb{E}\left[Z_{f,p}|\mathbf{y}\right] = \mathbb{E}_{\mathrm{gp}(f|\mathbf{y})}\left[\int f(\theta)p(\theta)d\theta\right] = \left[\int k(\theta, \theta_s)p(\theta)d\theta\right]\mathbf{K}^{-1}\mathbf{y} = \mathbf{z}^\mathsf{T}\mathbf{K}^{-1}\mathbf{y} \tag{A.5}$$

$$\mathbb{V}\left[Z_{f,p}|\mathbf{y}\right] = \mathbb{V}_{\mathrm{prior}}\left[Z_{f,p}\right] - \mathbf{z}^\mathsf{T}\mathbf{K}^{-1}\mathbf{z} \tag{A.6}$$

where

$$z_n = \int k(\theta, \theta_n)p(\theta)d\theta \tag{A.7}$$

$$\mathbb{V}_{\mathrm{prior}}\left[Z_{f,p}\right] = \iint k(\theta, \theta')p(\theta)p(\theta')d\theta d\theta'. \tag{A.8}$$

For longer derivations, see the supplementary material. This brings us to the one of the main technical constraints of this method: Choosing a form for the kernel function $k(\theta, \theta')$ such that we can compute (**??**) and (**??**) efficiently. We must also set or integrate out any parameters of k.

A.3.1 BQ as an inference method

If we assume that in (**??**), the form of $p(\theta)$ is such that we can compute z_n, then applying bq is straighforward. For example, in **?**, bq was used to solve problems where $p(\theta)$ was

a Gaussian prior over parameters, and $f(\theta) = p(x|\theta)$ was a likelihood function, making Z the *model evidence*, a useful quantity when comparing models.

Typically, however, we are also interested in other quantities besides the model evidence, such as marginal distributions of latent parameter. In that case, we must solve a more difficult integral, where $p(\theta) = p^*(\theta|x)$ is a possibly unnormalized distribution of unknown form.

$$\mathbb{E}_{p(\theta|\mathbf{x})}\left[f(\theta)\right] = \int f(\theta)p(\theta|x)d\theta \quad = \frac{1}{Z}\int f(\theta)p(x|\theta)p(\theta)d\theta \quad \text{where} \quad Z = \int p(x|\theta)p(\theta)d\theta \tag{A.9}$$

Integrals of this form can also be solved using Bayesian quadrature. For a thorough treatment of this problem, see [Mike's BQR paper].

This will show that bq can be applied in several ways: For instance, if we wish to perform inference about an unknown parameter τ, we can include it as a variable to be integrated over by the gp. However, if for some technical reason this is difficult, we can also simply vary our extra parameter over some range, recomputing $\mathbf{y}(\tau)$ and obtaining a marginal distribution over $Z_{f,p}$ for each value of τ. [Reference an experiment?] This approach is useful for post-hoc sensitivity analysis.

A.4 Guidelines for Constructing a Kernel

As pointed out above, one of the most important design decisions in bq is the choice of kernel function $k(\theta, \theta')$, which specifies the prior covariance between the values of the likelihood function $p(\mathbf{x}|\theta)$ and $p(\mathbf{x}|\theta')$. This function is somewhat analogous to the proposal distribution required to construct a Metropolis-Hastings sampler [cite]. In this section, we give guidance on how to construct an appropriate kernel.

The kernel typically should encode as much prior knowledge about the function being modeled as possible. In regression problems, this usually amounts to specifying the smoothness properties of the function being modeled. When doing inference, however, we typically know the likelihood function in closed form. The more properties of the likelihood function we can encode in the kernel, the fewer samples we will need in order to learn about the value of its integral. In particular, we should encode any known symmetries:

Symmetry Encoding: The prior correlation $\frac{k(\theta,\theta')}{\sqrt{k(\theta,\theta)}\sqrt{k(\theta',\theta')}}$ should equal 1 when $f(\theta) = f(\theta')$. That is to say, if two parameter settings are indistinguishable under the likelihood, our model can converge more quickly if it enforces that those likelihood values are identical. This is another way of saying that the covariance function should encode all known symmetries.

The ability to encode symmetries in the kernel is one of the major advantages of bq over Monte Carlo methods. In unidentifiable models such as mixture models, often it is known that there exist many symmeteric modes in the posterior, which represents a major difficulty when computing model evidence. By encoding these symmetries in the prior over likelihood functions, bq neatly solves the problem of identifiability when estimating $Z_{f,p}$.

A.4.1 Convergence

In the existing bq literature [cite only 4 papers], the integration problems considered have been low-dimensional, and the kernel function used has always been, to the best of the authors' knowledge, the squared-exponential kernel. In that case, existing results on the consistency of gp regression [cite consistency] imply that, under some conditions, the bq estimator (a linear transform of the gp posterior) is also consistent.

For infinite-dimnensional spaces with complex kernels, it is more difficult to prove consistency, although the known structure of the likelihood functions may help. In this section, we give conditions necessary for convergence.

First, the kernel must be positive-definite Rasmussen and Williams (2006). In addition, in order to ensure convergence, we must have that the following condition holds:

Identifiability: The prior correlation $\frac{k(\theta,\theta')}{\sqrt{k(\theta,\theta)}\sqrt{k(\theta',\theta')}}$ must be less than 1 if it is possible that $f(\theta) \neq f(\theta')$. That is to say, if two values of the likelihood function can be different, our model must not enforce that those two function values are identical.

Proposition 1. *The above condition is necessary to guarantee convergence of the BQ posterior to the true value of Z.*

Proof sketch. Consider a prior $p(\theta) = \frac{1}{2}\delta_{\theta_1}(\theta) + \frac{1}{2}\delta_{\theta_2}(\theta)$ where $\theta_1 \neq \theta_2$. If the prior correlation between $f(\theta_1)$ and $f(\theta_2)$ is one, then after observing one of those two values, say $f(\theta_1)$ we have that $\mathbb{E}_{\text{gp}}[Z] = f(\theta_1)$ and $\mathbb{V}_{\text{gp}}[Z] = 0$. However if $f(\theta_1) \neq f(\theta_2)$, then $Z_0 = \frac{1}{2}f(\theta_1) + \frac{1}{2}f(\theta_2) \neq f(\theta_1)$. Thus the estimator will have converged to the wrong hypothesis. □

For a more detailed proof, see the supplementary materical. The statements in this section also hold for the problem of gp regression in general, but are specially releveant for the problem of inferring likelihood functions over latent structures. This is for two reasons: First, likelihood functions over structures can typically by shown to have many symmetries. Secondly, in the quadrature setting, we must learn about the function everywhere under the prior, not just in a small region or manifold, as is typical for regression problems. Exploiting the symmetries of the likelihood function is both possible, and necessary for fast convergence.

A.5 Inference in the Indian Buffet Process

In this section, we construct a kernel and demonstrate the use of bq for inference in an infinite latent model, the Indian buffet process. The Indian buffet process (ibp) **?** is a distribution over binary matrices, usually used as a prior over latent features of a set of items. The ibp is nonparametric in the sense that the number of latent features is unbounded. For example, in **?**, a model of images is constructed where the entries of a binary matrix specify which objects appear in which images. Although the number of objects is unknown beforehand, given a set of images, the flexible ibp prior allows inference on both the number of objects, and their presence over the dataset.

Under an ibp prior, the probability of seeing a matrix $\mathbf{Z}$ with K columns is

$$P(\mathbf{Z}|\alpha) = \prod_{k=1}^{K} \frac{\frac{\alpha}{K}\Gamma(m_k + \frac{\alpha}{K})\Gamma(N - m_k + 1)}{\Gamma(N + 1 + \frac{\alpha}{K})} \tag{A.10}$$

where m_k is the number of ones in column k, and α is the concentration parameter. There is an unfortunate clash of notation here, where $Z_{f,p}$ denotes the model evidence, and $\mathbf{Z}$ is used to denote a binary matrix.

To fully specify a model, we must also specify the likelihood of a set of observations $\mathbf{X}$ given the latent structure, $p(\mathbf{X}|\mathbf{Z})$. For simplicity, we will use as a simple example the linear-Gaussian model from **?**. This model assumes the data is generated as $\mathbf{X} = \mathbf{A}\mathbf{Z} + \epsilon$, with $A_{ij} \sim \mathcal{N}(0, \sigma_A)$ and $\epsilon_{ij} \sim \mathcal{N}(0, \sigma_X)$. The features in $\mathbf{A}$ are turned on and off for each row of $\mathbf{X}$ by the entries of $\mathbf{Z}$. Conveniently, we can integrate out the matrix $\mathbf{A}$ to

obtain a collapsed likelihood:

$$p(\mathbf{X}|\mathbf{Z},\sigma_X,\sigma_A) = \frac{\exp\left\{-\frac{1}{2\sigma_X^2}\operatorname{tr}(\mathbf{X}^T(\mathbf{I}-\mathbf{Z}(\mathbf{Z}^T\mathbf{Z}+\frac{\sigma_X^2}{\sigma_A^2}\mathbf{E}_)^{-1}\mathbf{Z}^T)\mathbf{X})\right\}}{(2\pi)^{ND/2}\sigma_X^{(N-K)D}\sigma_A^{KD}|\mathbf{Z}^T\mathbf{Z}+\frac{\sigma_X^2}{\sigma_A^2}\mathbf{I}|^{\frac{D}{2}}} \tag{A.11}$$

The goal of inference in the ibp is usually do discover statistics about the matrices $\mathbf{Z}$ and $\mathbf{A}$, or to produce a predictive distribution over new rows of $\mathbf{X}$. In this paper, we will show how to [...]

A.5.1 A kernel between binary matrices

Here we give a kernel which satisfies the guidelines given in section **??**. Since the likelihood in (**??**) does not depend on the order of columns of $\mathbf{Z}$, we will construct a kernel function $k(\mathbf{Z},\mathbf{Z}')$ which is also invariant to permutations over columns of both $\mathbf{Z}$ and $\mathbf{Z}'$:

$$k(\mathbf{Z},\mathbf{Z}') = \sum_{k=1}^{K}\sum_{k'=1}^{K'}\sum_{n=1}^{N}\mathbf{Z}_{n,k}\mathbf{Z}'_{n,k'} \tag{A.12}$$

This kernel has the property that, for a given number of ones in $\mathbf{Z}$ and $\mathbf{Z}'$, it attains its maximum value when every element of some permutation of columns of $\mathbf{Z}$ is equal to $\mathbf{Z}'$ (i.e., they are in the same equivalence class). [TODO: show that it achieves identifiability condition]

A.5.2 Computing z_n and the prior variance

Now that we have defined our prior and kernel, we can compute the "mini-normalization constants", $z_1,\ldots,z_n$, given by (**??**). These quantities represent the expected covariance of the likelihood of a latent structure θ', with the likelihood of another structure drawn from the prior.

If matrices $\mathbf{Z}$ and $\mathbf{Z}'$ have K and K' columns respectively, then combining (**??**) and (**??**), we have:

$$z_n(\mathbf{Z}) = \sum_{\mathbf{Z}'}k(\mathbf{Z},\mathbf{Z}')p(\mathbf{Z}'|\alpha) = \sum_{\mathbf{Z}'}\left[\sum_{n=1}^{N}\sum_{k=1}^{K}\sum_{k'=1}^{K'}\mathbf{Z}_{n,k}\mathbf{Z}'_{n,k'}\right]\left[\prod_{k^*=1}^{K}P(\mathbf{Z}'_{:,k^*}|\alpha)\right] \tag{A.13}$$

$$= \sum_{k=1}^{K}\sum_{n=1}^{N}\mathbf{Z}_{n,k}\frac{\alpha}{1+\frac{\alpha}{K'}} = \alpha\sum_{k=1}^{K}\sum_{n=1}^{N}\mathbf{Z}_{n,k} \qquad \text{as } K'\to\infty \tag{A.14}$$

See the supplementary material for longer derivations. We can interpret (**??**) as saying that the prior covariance of the likelihood $p(\mathbf{X}|\mathbf{Z})$ with a randomly drawn likelihood $p(\mathbf{X}|\mathbf{Z}')$ is proportional to the number of ones in $\mathbf{Z}$.

Next we compute the prior variance (**??**), which follows a similar derivation. This is the expected variance of Z before we have seen any data.

$$V_{\text{prior}} = \sum_{\mathbf{Z}'} \sum_{\mathbf{Z}} p(\mathbf{Z}|\alpha) k(\mathbf{Z}, \mathbf{Z}') p(\mathbf{Z}'|\alpha) = \frac{\alpha^2 N}{1 + \frac{\alpha}{K}} = \alpha^2 N \qquad \text{as } K \to \infty \tag{A.15}$$

This form is intuitive: it scales with the expected number of ones per row, α. As α or N approach zero, the likelihood surface can be expected to become less varied, since there will be fewer ways that individual samples of $\mathbf{Z}$ can differ.

A.6 Infinite Mixture Models

In this section we develop a more general example, placing a kernel between mixture distributions. This will allow us to perform model-based inference in Dirichlet process mixture models.

A finite mixture model with k components gives a distribution over the observations x as follows: $p(x|\pi, \theta) = \sum_{i=1}^{k} \pi_i p(x|\theta_i)$ where θ_i represents a single set of mixture parameters. By specifying the form of θ, we can perform inference in a wide variety of infinite mixture models, such as an latent Dirichlet allocation-type model, infinite mixture of regressors, or a mixture of Gaussians.

We will divide our derivation into two parts. First, we will define a kernel between multinomial distributions, and derive (**??**) and (**??**) for this kernel, leaving unspecified the kernel between individual mixture elements. Then, we will continue the derivation for an infinite mixture of Gaussians.

A.6.1 A Kernel Between Multinomial Distributions

Here we define a kernel between multinomial distributions, possibly of different dimension. Here, π represents weights which sum to one, and θ the atoms of the multinomial distribution.

$$k(\pi, \theta, \pi', \theta') = \sum_{i}^{n_\theta} \sum_{j}^{n_{\theta'}} \pi_i \pi'_j k_a(\theta_i, \theta'_j) \tag{A.16}$$

where $k_a(\theta, \theta')$ specifies the covariance between individual atoms of the distribution. Changing the order of mixture components, or splitting a given mixture component among two identical atoms, will not affect the value of this covariance function. If $k_a(\theta_i, \theta'_j)$ is a Mercer kernel, then so is (**??**).

If our mixture θ has n_θ components, then

$$z(\pi, \theta) = \iint k(\pi, \theta, \pi', \theta') p(\theta') p(\pi') d\theta' d\pi' = \iint \left[\sum_{i=1}^{n_\theta} \sum_{j=1}^{n_{\theta'}} \pi_i \pi'_j k(\theta_i, \theta'_j) \right] \left[\prod_a p(\theta'_a) \right] p(\pi') d\theta' d\pi'$$

$$= \int \sum_{i=1}^{n_\theta} \sum_{j=1}^{n_{\theta'}} \pi_i \pi'_j \underbrace{\int k(\theta_i, \theta'_j) p(\theta'_j) d\theta'_j}_{z_a(\theta_i)} p(\pi') d\pi' = \sum_{i=1}^{n_\theta} \pi_i z_a(\theta_i) \tag{A.17}$$

$$\mathbb{V}_{\text{prior}}[Z_{f,p}] = \iint z(\pi, \theta) p(\theta) p(\pi) d\theta d\pi = \underbrace{\int z(\theta_i) p(\theta_i) d\theta_i}_{V_a} \underbrace{\int p(\pi) \sum_{i=1}^{n_\theta} \pi_i d\pi}_{\text{sums to one}} = V_a \tag{A.18}$$

where $V_a = \iint p(\theta) k_a(\theta, \theta') p(\theta') d\theta' d\theta$ is the prior variance of k_a, which will be defined below.

Perhaps surprisingly, neither z_n nor V_{prior} depend on the number of proposed mixture components. This means that we are free to take the infinite limit $n_\theta \to \infty$. Perhaps this makes sense: The likelihood does not change if we divide up our clusters to give equivalent mixtures but having more components. These quantities also do not depend on the form of the prior over mixture components $p(\pi)$, nor the prior over individual components $p(\theta)$, as long as it factorizes over components.

A.6.2 Infinite Mixture of Gaussians

The above kernel between mixtures can be used for inference in a wide variety of infinite mixture models. For simplicity, in this paper we will use as an example the infinite mixture of Gaussians **?**:

$$p(x|\pi, \theta) = \sum_{i=1}^{k} \pi_i p(x|\theta_i) = \sum_{i=1}^{k} \pi_i \mathcal{N}(y|\mu_i, \Sigma_i) \tag{A.19}$$

where $\theta_i = \{\mu_i, \Sigma_i\}$ represent the parameters of a single Gaussian. To complete our example, all that remains is to specify a kernel k_a between individual mixture components, and to compute z_k and V_a. For simplicity, we will specify a Gaussian kernel between

densities, and assume that the variance of each mixture component is identical:

$$k(\mu, \Sigma, \mu', \Sigma') = \mathcal{N}(\mu|\mu', \Sigma_k) \tag{A.20}$$

where the entries of Σ_k are kernel parameters. Next, we give (**??**) and (**??**) for this kernel:

$$z_k(\mu_i, \Sigma_i) = \iint k(\mu_i, \Sigma_i, \mu'_j, \Sigma'_j) p(\mu'_j, \Sigma'_j) d\mu'_j d\Sigma'_j = \mathcal{N}(\mu_i|\lambda, \Sigma_k + \Sigma_p) \tag{A.21}$$

$$V_a = \int z_k(\mu_i, \Sigma_i) p(\mu_i, \Sigma_i) d\mu_i d\Sigma_i = \mathcal{N}(0|0, \Sigma_k + 2\Sigma_p) \tag{A.22}$$

Note that the prior variance V_k depends only on the shape of the prior Σ_p, and not its location.

A.7 Related Work

String kernels **?**. Graph kernels. Tree-structured kernels. Sequence kernels. A review of kernels in structured domains can be found in **?**.

A.8 Experiments

Integrating Kernel Hyperparameters One complicating issue of inference using bq is how to set kernel hyperparameters. In **?**, these were set by maximum likelihood. In our experiments, hyperparameters were integrated out numerically, except for the *output variance* (a scale factor in front of the kernel) which is possible to integrate out in closed form, giving a final posterior variance of $\sigma_2 = \frac{1}{N} [\mathbf{y}^t \mathbf{K}^{-1} \mathbf{y}] [V_k - \mathbf{z}_t \mathbf{K}^{-1} \mathbf{z}]$. For a derivation, see the supplementary material.

A.8.1 IBP Experiments

We used collapsed IBP sampling code from **?** to obtain samples and likelihood values. We used data from **?**, where the true value of $\sigma_x = 0.5$. We set the number of datapoints to be small (N = 25), since this is a regime where VB is known to perform poorly **?**.

Figure **??** demonstrates the use of bq, showing that a set of samples gathered under one parameter setting can be used to make inferences the likelihood of other parameter settings. This allows us to use incorrect samplers, use samples from the burn-in period,

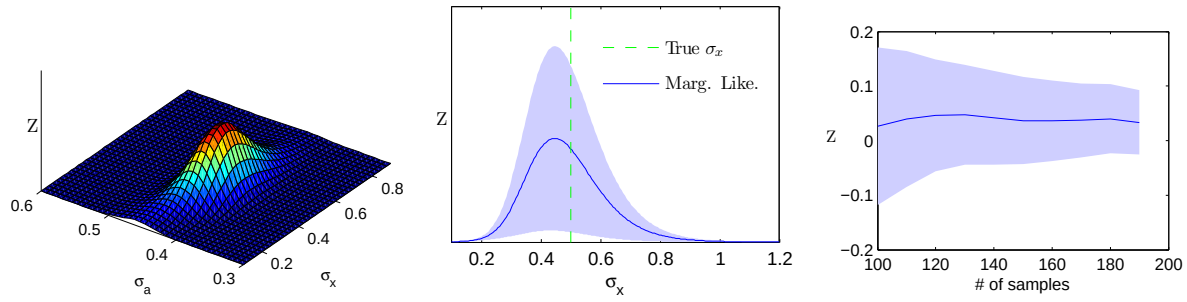

Fig. A.2 Computing marginal likelihoods with BQ. Left: The marginal likelihood as a function of two nuisance parameters. Center: A slice of the 2-D marginal likelihood function, at $\sigma_A = 0.4$. The true value of σ_X lies roughly in the center of the likelihood function. Right: The marginal likelihood as a function of the number of evaluations of the likelihood function. The shaded error represents uncertainty about the value of the marginal likelihood.

etc. For example, the likelihood function (**??**) has two "nuisance parameters", σ_X and σ_A. In [cite Finale], these parameters are simply set in an ad-hoc way. This may be acceptable, but using MCMC, it is not clear how to tell whether the answer is sensitive to these nuisance parameters without re-running the chain under several different settings. Figure **??** shows that bq allows one to run a post-hoc sensitivity analysis to check whether extra parameters are important to the analysis. In addition, we recover an estimate of the certainty of our analysis, indicating whether or not the existing samples are sufficient to draw strong conclusions.

A.8.2 DP Mixture Experiments

Figure **??** demonstrates the use of bq to examine sensitivity to prior parameters.

Figures **??** and **??** show not only the marginal likelihood of different parameter settings, but also the marginal variance of the likelihood functions. We must distinguish between two types of uncertainty represented here. First, the shape of the likelihood function indicates our posterior uncertainty over its parameter, given the data. Second, the gp posterior uncertainty in the likelihood function(represented by the shaded areas) represents our uncertainty about this likelihood function. Our uncertainty about the likelihood function can be made arbitrarily small by continuing to sample the likelihood function. However, we may still remain uncertain about the value of the latent parameter.

Code to produce all experiments will be made available at the authors' website.

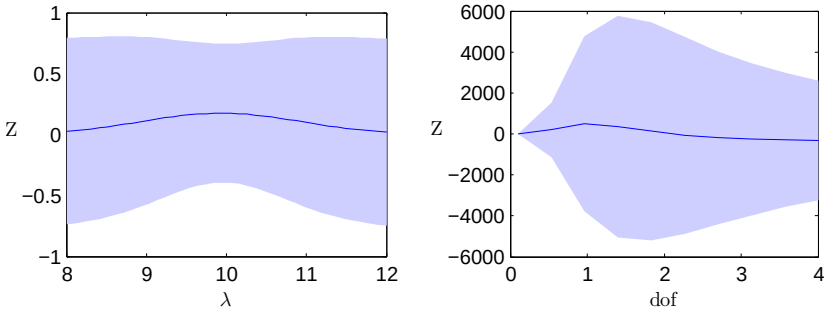

Fig. A.3 A demonstration of computing marginal likelihoods. Left: The marginal likelihood versus the prior mean. Right: Marginal likelihood versus the degrees of freedom of the mixture components. dof $= 1$ is Cauchy, dof $= 2$ is Student's t, dof $= \infty$ is Gaussian. The shaded error represents uncertainty about the value of the marginal likelihood.

A.9 Discussion

Nuisance parameters such as σ_X could also be dealt with in the bq by adding them to the kernel and the domain of integration if desired.

A.9.1 Appropriateness of the GP prior

Placing a gp prior on the likelihood function allows us to take advantage of our knowledge of the smoothness of this function. However, there is ample reason to be believe that the gp prior is inappropriate for modeling likelihood functions. In **?** it is suggested to place the gp on the log-likelihood function, which would presumably make the additive form of the kernels given in the paper much more appropriate. This was done by [cite BQR paper], and resulted in better performance, at the cost of a much more complicated inference procedure.

As is generally true for Bayesian methods, there exist many cases where bq will underestimate its uncertainty. Our response to this objection is that any uncertainty estimate is better than none at all. In our experiments, we observed cases in which the model's posterior uncertainty is significant, alerting us to the fact that we have not yet observed enough about the likelihood function to be certain about its shape. In the case of MCMC, this sort of uncertainty estimate is typically unavailable. That is to say, our model cannot account for 'unknown unknowns', but it can at least account for 'known unknowns', which is a step up from the point estimates provided by MCMC.

A.10 Conclusions

We have extended Bayesian quadrature to infinite, structured domains, and demonstrated that this method can be used for inference in nonparametric models. We have given necessary conditions for convergence and examples of how to construct kernels which take advantage of the many symmetries of typical likelihood functions. We demonstrated some properties of this method, which include uncertainty estimates, flexibility in sampling methods, and the ability to re-use samples from on setting to perform post-hoc sensitivity analysis of nuisance parameters.

Appendix B

Characterizing Deep Gaussian Process Models

> "On a given day, would I rather be wrestling with a sampler, or proving theorems?"
>
> *Peter Orbanz*, personal communication

Choosing appropriate architectures and regularization strategies of deep networks is crucial to good predictive performance. To shed light on this problem, we analyze the analogous problem of constructing useful priors on compositions of functions. Specifically, we study the deep Gaussian process, a type of infinitely-wide, deep neural network. We show that in standard architectures, the representational capacity of the network tends to capture fewer degrees of freedom as the number of layers increases, retaining only a single degree of freedom in the limit. We propose an alternate network architecture which does not suffer from this pathology. We also examine deep covariance functions, obtained by composing infinitely many feature transforms. Lastly, we characterize the class of models obtained by performing dropout on Gaussian processes.

This chapter was joint work with Oren Rippel, Ryan P. Adams and Zoubin Ghahramani.

B.1 Introduction

Much recent work on deep networks has focused on weight initialization (Martens, 2010), regularization (Lee et al., 2007) and network architecture (Gens and Domingos, 2013). However, the interactions between these different design decisions can be complex and

difficult to characterize. We propose to approach the design of deep architectures by examining the problem of assigning priors to nested compositions of functions. Well-defined priors allow us to explicitly examine the assumptions being made about functions we may wish to learn. If we can identify classes of priors that give our models desirable properties, these in turn may suggest regularization, initialization, and architecture choices that also provide such properties.

Fundamentally, a multilayer neural network implements a composition of vector-valued functions, one per layer. Hence, understanding properties of such function compositions helps us gain insight into deep networks. In this paper, we examine a simple and flexible class of priors on compositions of functions, namely deep Gaussian processes (Damianou and Lawrence, 2013). Deep gps are simply priors on compositions of vector-valued functions, where each output of each layer is drawn independently from a GP prior:

$$\mathbf{f}^{(1:L)}(\mathbf{x}) = \mathbf{f}^{(L)}(\mathbf{f}^{(L-1)}(\dots \mathbf{f}^{(2)}(\mathbf{f}^{(1)}(\mathbf{x}))\dots)) \tag{B.1}$$

$$\mathbf{f}_d^{(\ell)} \overset{\text{ind}}{\sim} \text{gp}\left(0, k_d^{\ell}(\mathbf{x}, \mathbf{x}')\right) \tag{B.2}$$

These models correspond to a certain type of infinitely-wide multi-layer perceptron (MLP), and as such make canonical candidates for generative models of functions that closely relate to neural networks.

By characterizing these models, this paper shows that representations based on repeated composition of independently-initialized functions exhibit a pathology where the representation becomes invariant to all but one direction of variation. This corresponds to an eventual debilitating decrease in the information capacity of networks as a function of their number of layers. However, we will demonstrate that a simple change in architecture — namely, connecting the input to each layer — fixes this problem.

We also present two related analyses: first, we examine the properties of a arbitrarily deep fixed feature transforms ("deep kernels"). Second, we characterise the prior obtained by performing dropout on gps, showing equivalences to existing models.

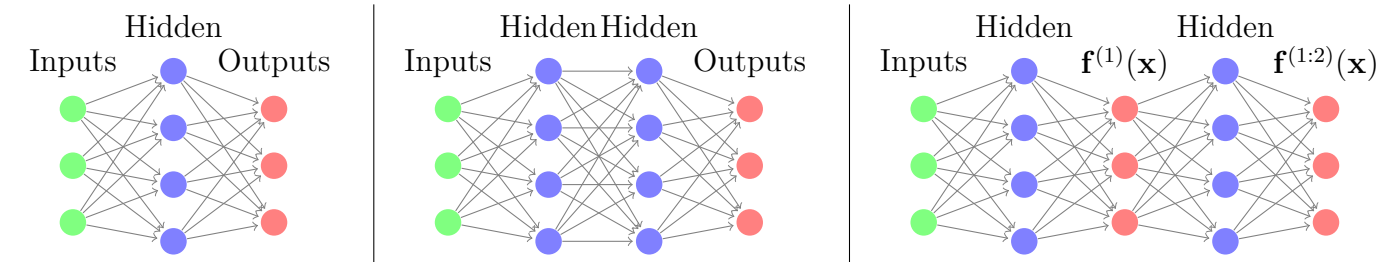

a) One-hidden-layer MLP b) Two-hidden layer MLP c) Two-layer gp: $\mathbf{y} = \mathbf{f}^{(2)}\left(\mathbf{f}^{(1)}(\mathbf{x})\right)$

Fig. B.1 GPs can be understood as one-hidden-layer MLP with infinitely many hidden units (a). There are two possible interpretations of deep GPs: We can consider the deep GP to be a neural network with a finite number of hidden units, each with a different non-parametric activation function (b). Alternatively, we can consider every second layer to be a random linear combination of an infinite number of fixed parametric hidden units (c).

B.2 Relating deep neural nets and deep Gaussian processes

B.2.1 Single-layer models

In the typical definition of an MLP, the hidden units of the first layer are defined as:

$$\mathbf{h}^{(1)}(\mathbf{x}) = \sigma\left(\mathbf{b}^{(1)} + \mathbf{W}^{(1)}\mathbf{x}\right) \tag{B.3}$$

where $\mathbf{h}$ are the hidden unit activations, $\mathbf{b}$ is a bias vector, $\mathbf{W}$ is a weight matrix and σ is a one-dimensional nonlinear function applied element-wise. The output vector $f(\mathbf{x})$ is simply a weighted sum of these hidden unit activations:

$$f(\mathbf{x}) = \mathbf{V}^{(1)}\sigma\left(\mathbf{b}^{(1)} + \mathbf{W}^{(1)}\mathbf{x}\right) = \mathbf{V}^{(1)}\mathbf{h}^{(1)}(\mathbf{x}) \tag{B.4}$$

where $\mathbf{V}^{(1)}$ is another weight matrix.

There exists a correspondence between one-layer MLPs and gps (Neal, 1995). gps can be viewed as a prior on neural networks with infinitely many hidden units, and unknown weights. More precisely, for any model of the form

$$f(\mathbf{x}) = \frac{1}{K}\alpha^{\mathsf{T}}\mathbf{h}(\mathbf{x}) = \frac{1}{K}\sum_{i=1}^{K}\alpha_i h_i(\mathbf{x}), \tag{B.5}$$

with fixed features $[h_1(\mathbf{x}), \ldots, h_K(\mathbf{x})]^{\mathsf{T}} = \mathbf{h}(\mathbf{x})$ and i.i.d. α's with zero mean and fi-

nite variance σ^2, the central limit theorem implies that as the number of features K grows, any two function values $f(\mathbf{x}), f(\mathbf{x}')$ have a joint distribution approaching $\mathcal{N}\left(0, \frac{\sigma^2}{K}\sum_{i=1}^{K} h_i(\mathbf{x})h_i(\mathbf{x}')\right)$. A joint Gaussian distribution between any set of function values is the definition of a Gaussian process.

The result is surprisingly general: it puts no constraints on the features (other than having uniformly bounded activation), nor does it require that the feature weights α be Gaussian distributed.

We can also work backwards to derive a one-layer MLP from any gp. Mercer's theorem implies that any positive-definite kernel function corresponds to an inner product of features: $k(\mathbf{x}, \mathbf{x}') = \mathbf{h}(\mathbf{x})^\mathsf{T}\mathbf{h}(\mathbf{x}')$. Thus in the one-hidden-layer case, the correspondence between MLPs and gps is simple: the features $\mathbf{h}(\mathbf{x})$ of the kernel correspond to the hidden units of the MLP.

B.2.2 Multiple hidden layers

In an MLP, the ℓth layer units are given by the recurrence

$$\mathbf{h}^{(\ell)}(\mathbf{x}) = \sigma\left(\mathbf{b}^{(\ell)} + \mathbf{W}^{(\ell)}\mathbf{h}^{(\ell-1)}(\mathbf{x})\right) . \tag{B.6}$$

This architecture is shown in figure A.1b. For example, if we extend the model given by (A.4) to have two layers of feature mappings, the resulting model is

$$f(\mathbf{x}) = \frac{1}{K}\alpha^\mathsf{T}\mathbf{h}^{(2)}\left(\mathbf{h}^{(1)}(\mathbf{x})\right) . \tag{B.7}$$

If the features $\mathbf{h}(\mathbf{x})$ are considered fixed with only the last layer weights α unknown, this model corresponds to a gp with a "deep kernel":

$$k(\mathbf{x}, \mathbf{x}') = \left(\mathbf{h}^{(2)}(\mathbf{h}^{(1)}(\mathbf{x}))\right)^\mathsf{T}\mathbf{h}^{(2)}(\mathbf{h}^{(1)}(\mathbf{x}')) \tag{B.8}$$

These models, examined in section A.6, imply a fixed representation as opposed to a prior over representations, which is what we wish to analyze in this paper.

To construct a neural network with fixed nonlinearities corresponding to a deep gp, one must introduce a second layer in between each infinitely-wide set of fixed basis functions, as in figure A.1c. The D_ℓ outputs $\mathbf{f}^{(\ell)}(\mathbf{x})$ in between each layer are weighted sums (with unknown weights) of the fixed hidden units of the layer below, and the next layer's hidden units depend only on these D_ℓ outputs.

This alternating-layer architecture has an interpretation as a series of linear information bottlenecks. We can simply substitute (A.4) into (A.6) to get

$$\mathbf{h}^{(\ell)}(\mathbf{x}) = \sigma\left(\mathbf{b}^{(\ell)} + \mathbf{W}^{(\ell)}\mathbf{V}^{(\ell-1)}\mathbf{h}^{(\ell-1)}(\mathbf{x})\right) . \tag{B.9}$$

Thus, ignoring the intermediate outputs $\mathbf{f}^{(\ell)}(\mathbf{x})$, a deep gp is an infinitely-wide, deep MLP with each pair of layers connected by random, rank-D_ℓ matrices $\mathbf{W}^{(\ell)}\mathbf{V}^{(\ell-1)}$.

A more direct way to construct a network architecture corresponding to a deep gp is to integrate out all $\mathbf{V}^{(\ell)}$, and view deep gps as a neural network with a finite number of nonparametric, gp-distributed basis functions at each layer, in which $\mathbf{f}^{(1:\ell)}(\mathbf{x})$ represent the output of the hidden nodes at the ℓ^{th} layer. This second view lets us compare deep gp models to standard neural net architectures more directly.

B.3 Characterizing deep Gaussian processes

In this section, we develop several theoretical results that explore the behavior of deep gps as a function of their depth. This will allow us in section A.4 to formally identify a pathology that emerges in very deep networks.

Specifically, we will show that the size of the derivative of a one-dimensional deep gp becomes log-normal distributed as the network becomes deeper. We'll also show that the Jacobian of a multivariate deep gp is a product of independent Gaussian matrices with independent entries.

B.3.1 One-dimensional asymptotics

In this section, we derive the limiting distribution of the derivative of an arbitrarily deep, one-dimensional gp with a squared-exp kernel:

$$k_{\text{SE}}(x, x') = \sigma^2 \exp\left(\frac{-(x-x')^2}{2w^2}\right) . \tag{B.10}$$

The hyperparameter σ^2 controls the variance of functions drawn from the prior, and the hyperparameter w controls the smoothness. The derivative of a gp with a squared-exp kernel is pointwise distributed as $\mathcal{N}(0, \sigma^2/w^2)$. Intuitively, a gp is likely to have large derivatives if it has high variance and small lengthscales.

By the chain rule, the derivative of a one-dimensional deep gp is simply a product of its (independent) derivatives. The distribution of the absolute value of this derivative is

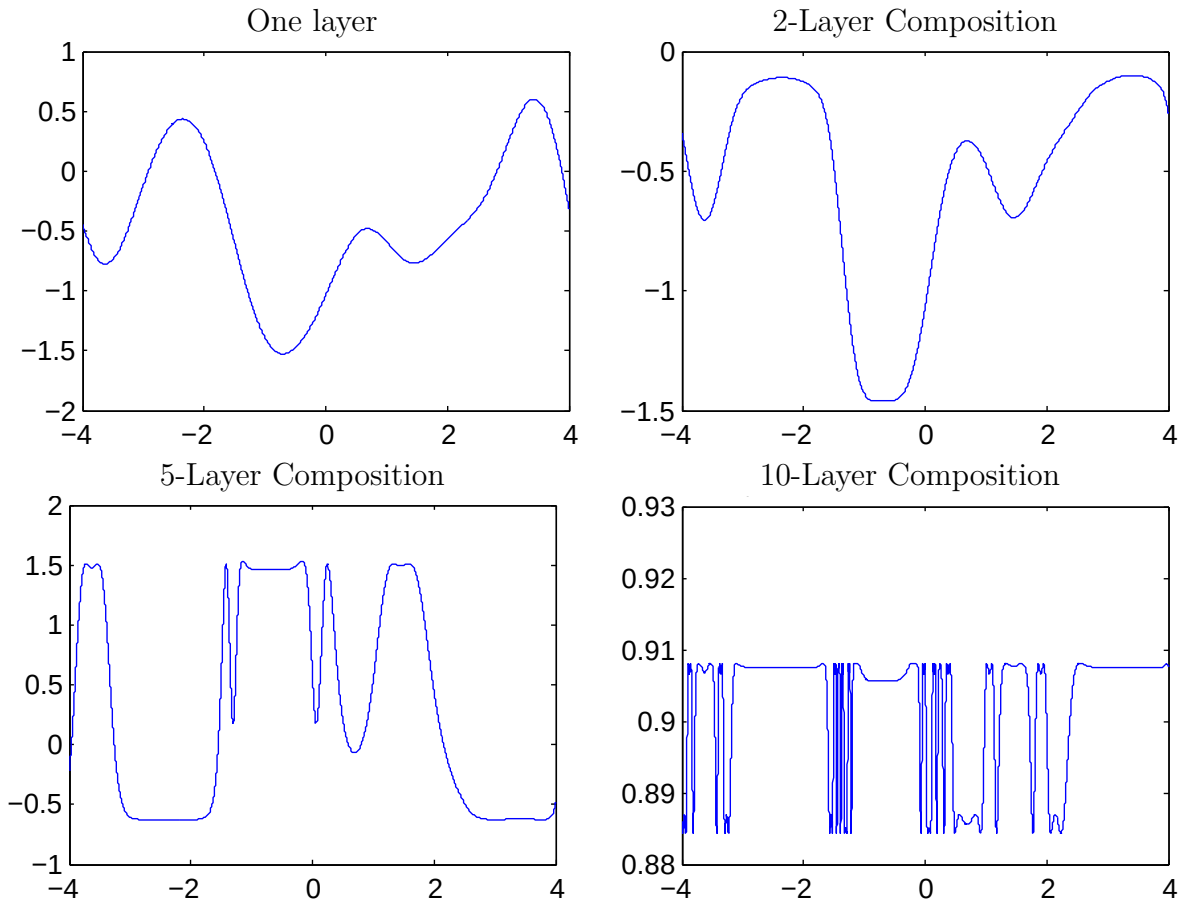

Fig. B.2 One-dimensional draws from a deep GP prior. After a few layers, the functions begin to be either nearly flat, or highly varying, everywhere. This is a consequence of the distribution on derivatives becoming heavy-tailed.

a product of half-normals, each with mean $\sqrt{2\sigma^2/\pi w^2}$.

If we choose kernel parameters so that $\sigma^2/w^2 = \pi/2$, then the expected magnitude of the derivative remains constant regardless of the depth.

The log of the magnitude of the derivatives has moments

$$\begin{aligned} m_{\log} &= \mathbb{E}\left[\log\left|\frac{\partial f(x)}{\partial x}\right|\right] = 2\log\left(\frac{\sigma}{w}\right) - \log 2 - \gamma \\ v_{\log} &= \mathbb{V}\left[\log\left|\frac{\partial f(x)}{\partial x}\right|\right] = \frac{\pi^2}{4} + \frac{\log^2 2}{2} - \gamma^2 - \gamma\log 4 \\ &\quad + 2\log\left(\frac{\sigma}{w}\right)\left[\gamma + \log 2 - \log\left(\frac{\sigma}{w}\right)\right] \end{aligned} \tag{B.11}$$

where $\gamma \approxeq 0.5772$ is Euler's constant. Since the second moment is finite, by the central limit theorem, the limiting distribution of the size of the gradient approaches log-normal as L grows:

$$\begin{aligned} \log\left|\frac{\partial f^{(1:L)}(x)}{\partial x}\right| &= \sum_{\ell=1}^{L} \log\left|\frac{\partial f^{(\ell)}(x)}{\partial x}\right| \\ \implies \log\left|\frac{\partial f^{(1:L)}(x)}{\partial x}\right| &\overset{L\to\infty}{\sim} \mathcal{N}\left(Lm_{\log}, L^2 v_{\log}\right) \end{aligned} \tag{B.12}$$

Even if the expected magnitude of the derivative remains constant, the variance of the log-normal distribution grows without bound as the depth increases. Because the log-normal distribution is heavy-tailed and its domain is bounded below by zero, the derivative will become very small almost everywhere, with rare but very large jumps.

Figure A.2 shows this behavior in a draw from a 1D deep gp prior, at varying depths. This figure also shows that once the derivative in one region of the input space becomes very large or very small, it is likely to remain that way in subsequent layers.

B.3.2 Distribution of the Jacobian

We now derive the distribution on Jacobians of multivariate functions drawn from a deep gp prior.

Lemma B.3.1. *The partial derivatives of a function mapping $\mathbb{R}^D \to \mathbb{R}$ drawn from a gp prior with a product kernel are independently Gaussian distributed.*

Proof. Because differentiation is a linear operator, the derivatives of a function drawn from a gp prior are also jointly Gaussian distributed. The covariance between partial

derivatives w.r.t. input dimensions d_1 and d_2 of vector $\mathbf{x}$ are given by Solak et al. (2003):

$$\operatorname{cov}\left(\frac{\partial f(\mathbf{x})}{\partial x_{d_1}}, \frac{\partial f(\mathbf{x})}{\partial x_{d_2}}\right) = \left.\frac{\partial^2 k(\mathbf{x}, \mathbf{x}')}{\partial x_{d_1} \partial x'_{d_2}}\right|_{\mathbf{x}=\mathbf{x}'} \tag{B.13}$$

If our kernel is a product over individual dimensions $k(\mathbf{x}, \mathbf{x}') = \prod_d^D k_d(x_d, x'_d)$, as in the case of the squared-exp kernel, then the off-diagonal entries are zero, implying that all elements are independent. □

In the case of the multivariate squared-exp kernel, the covariance between derivatives has the form:

$$\begin{aligned} f(\mathbf{x}) &\sim \mathrm{GP}\left(0, \sigma^2 \prod_{d=1}^{D} \exp\left(-\frac{1}{2}\frac{(x_d - x'_d)^2}{w_d^2}\right)\right) \\ \implies \operatorname{cov}\left(\frac{\partial f(\mathbf{x})}{\partial x_{d_1}}, \frac{\partial f(\mathbf{x})}{\partial x_{d_2}}\right) &= \begin{cases} \frac{\sigma^2}{w_{d_1}^2} & \text{if } d_1 = d_2 \\ 0 & \text{if } d_1 \neq d_2 \end{cases} \end{aligned} \tag{B.14}$$

Lemma B.3.2. *The Jacobian of a set of D functions $\mathbb{R}^D \to \mathbb{R}$ drawn independently from a gp prior with a product kernel is a $D \times D$ matrix of independent Gaussian R.V.'s*

Proof. The Jacobian of the vector-valued function $\mathbf{f}(\mathbf{x})$ is a matrix J with elements $J_{ij} = \frac{\partial \mathbf{f}_i(\mathbf{x})}{\partial x_j}$. Because we've assumed that the gps on each output dimension $\mathbf{f}_d(\mathbf{x})$ are independent (A.2), it follows that each row of J is independent. Lemma A.3.1 shows that the elements of each row are independent Gaussian. Thus all entries in the Jacobian of a gp-distributed transform are independent Gaussian R.V.'s. □

Theorem B.3.3. *The Jacobian of a deep gp with a product kernel is a product of independent Gaussian matrices, with each entry in each matrix being drawn independently.*

Proof. When composing L different functions, we'll denote the *immediate* Jacobian of the function mapping from layer $\ell - 1$ to layer ℓ as $J^\ell(\mathbf{x})$, and the Jacobian of the entire composition of L functions by $J^{1:L}(\mathbf{x})$. By the multivariate chain rule, the Jacobian of a composition of functions is simply the product of the immediate Jacobian matrices of each function. Thus the Jacobian of the composed (deep) function $\mathbf{f}^{(L)}(\mathbf{f}^{(L-1)}(\ldots \mathbf{f}^{(3)}(\mathbf{f}^{(2)}(\mathbf{f}^{(1)}(\mathbf{x})))\ldots))$ is

$$J^{1:L}(\mathbf{x}) = J^L J^{(L-1)} \ldots J^3 J^2 J^1. \tag{B.15}$$

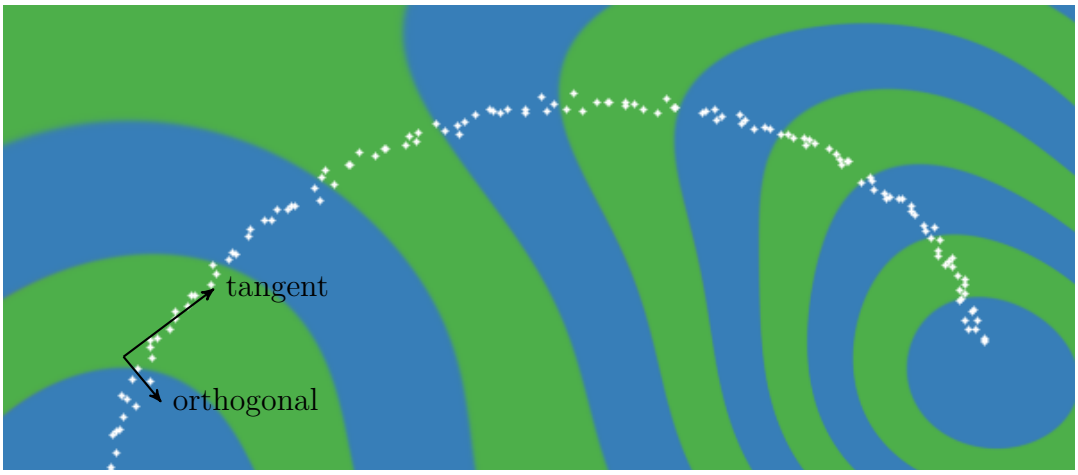

Fig. B.3 Representing a 1-D manifold. Colors show the output of the computed representation as a function of the input space. The representation (blue & green) is invariant in directions orthogonal to the data manifold (white), making it robust to noise in those directions, and reducing the number of parameters needed to represent a datapoint. The representation also changes in directions tangent to the manifold, preserving information for later layers.

By lemma A.3.2, each $J_{i,j}^{\ell} \overset{\text{ind}}{\sim} \mathcal{N}$, so the complete Jacobian is a product of independent Gaussian matrices, with each entry of each matrix drawn independently. □

Theorem A.3.3 allows us to analyze the representational properties of a deep Gaussian process by simply examining the properties of products of independent Gaussian matrices, a well-studied object.

B.4 Formalizing a pathology

Rifai et al. (2011a) argue that a good latent representation is invariant in directions orthogonal to the manifold on which the data lie. Conversely, a good latent representation must also change in directions tangent to the data manifold, in order to preserve relevant information. Figure A.3 visualizes this idea. We follow Rifai et al. (2011b) in characterizing the representational properties of a function by the singular value spectrum of the Jacobian. In their experiments, the Jacobian was computed at the training points. Because the priors we are examining are stationary, the distribution of the Jacobian is identical everywhere. Figure A.4 shows the singular value spectrum for 5-dimensional deep GPs of different depths. As the net gets deeper, the largest singular value dominates, implying there is usually only one effective degree of freedom in representation being computed.

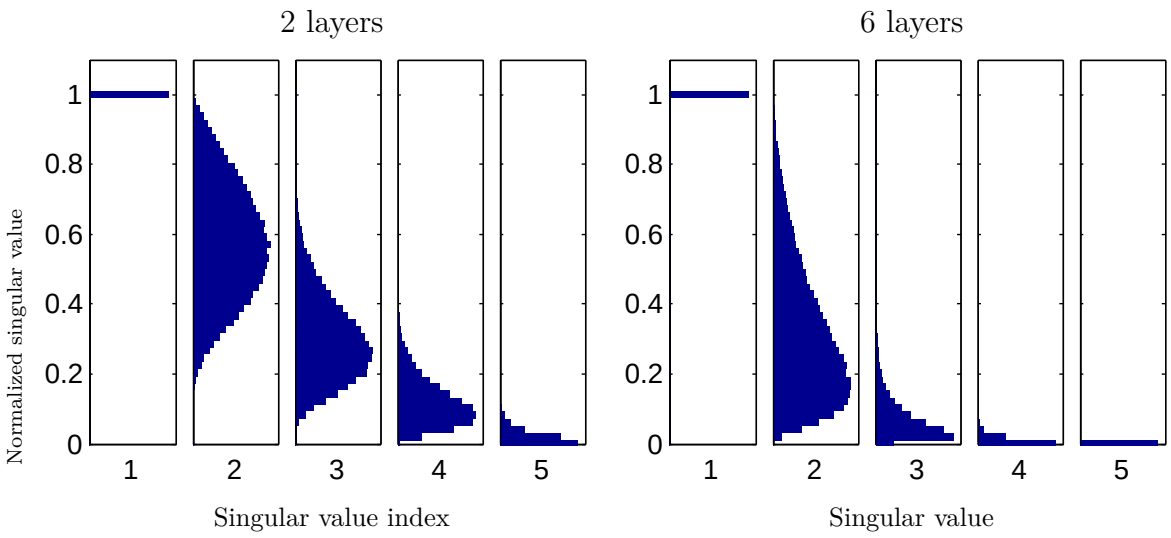

Fig. B.4 The normalized singular value spectrum of the Jacobian of a deep GP. As the net gets deeper, the largest singular value dominates. This implies that with high probability, there is only one effective degree of freedom in the representation being computed.

Figure A.5 demonstrates a related pathology that arises when composing functions to produce a deep density model. The density in the observed space eventually becomes locally concentrated onto one-dimensional manifolds, or *filaments*, implying that such models are insuitable to model manifolds whose underlying dimensionality is greater than one.

To visualize this pathology in another way, figure A.6 illustrates a colour-coding of the representation computed by a deep gp, evaluated at each point in the input space. After 10 layers, we can see that locally, there is usually only one direction that one can move in $\mathbf{x}$-space in order to change the value of the computed representation. This means that such representations are likely to be unsuitable for decision tasks that depend on more than one property of the input.

To what extent are these pathologies present in nets being used today? In simulations, we found that for deep functions with a fixed latent dimension D, the singular value spectrum remained relatively flat for hundreds of layers as long as $D > 100$. Thus, these pathologies are unlikely to severely affect relatively shallow, wide networks.

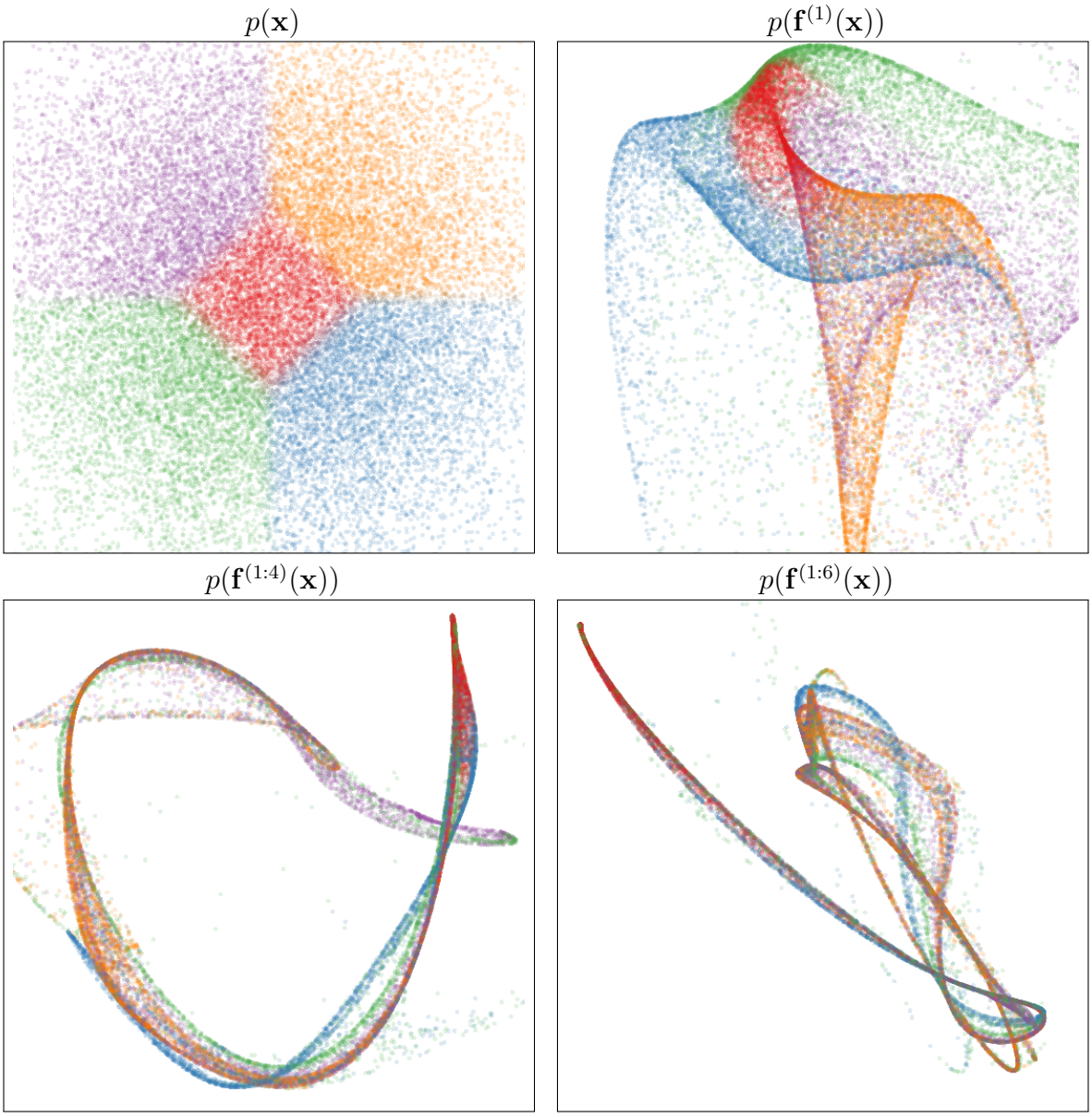

Fig. B.5 Visualization of draws from a deep GP. A 2-dimensional Gaussian distribution (top left) is warped by successive functions drawn from a GP prior. As the number of layers increases, the density concentrates along one-dimensional filaments.

B.5 Fixing the pathology

Following a suggestion from Neal (1995), we can fix the pathologies exhibited in figures A.5 and A.6 by simply making each layer depend not only on the output of the previous layer, but also on the original input $\mathbf{x}$. We refer to these models as *input-connected* networks. Figure A.7 shows a graphical representation of the two connectivity architec-

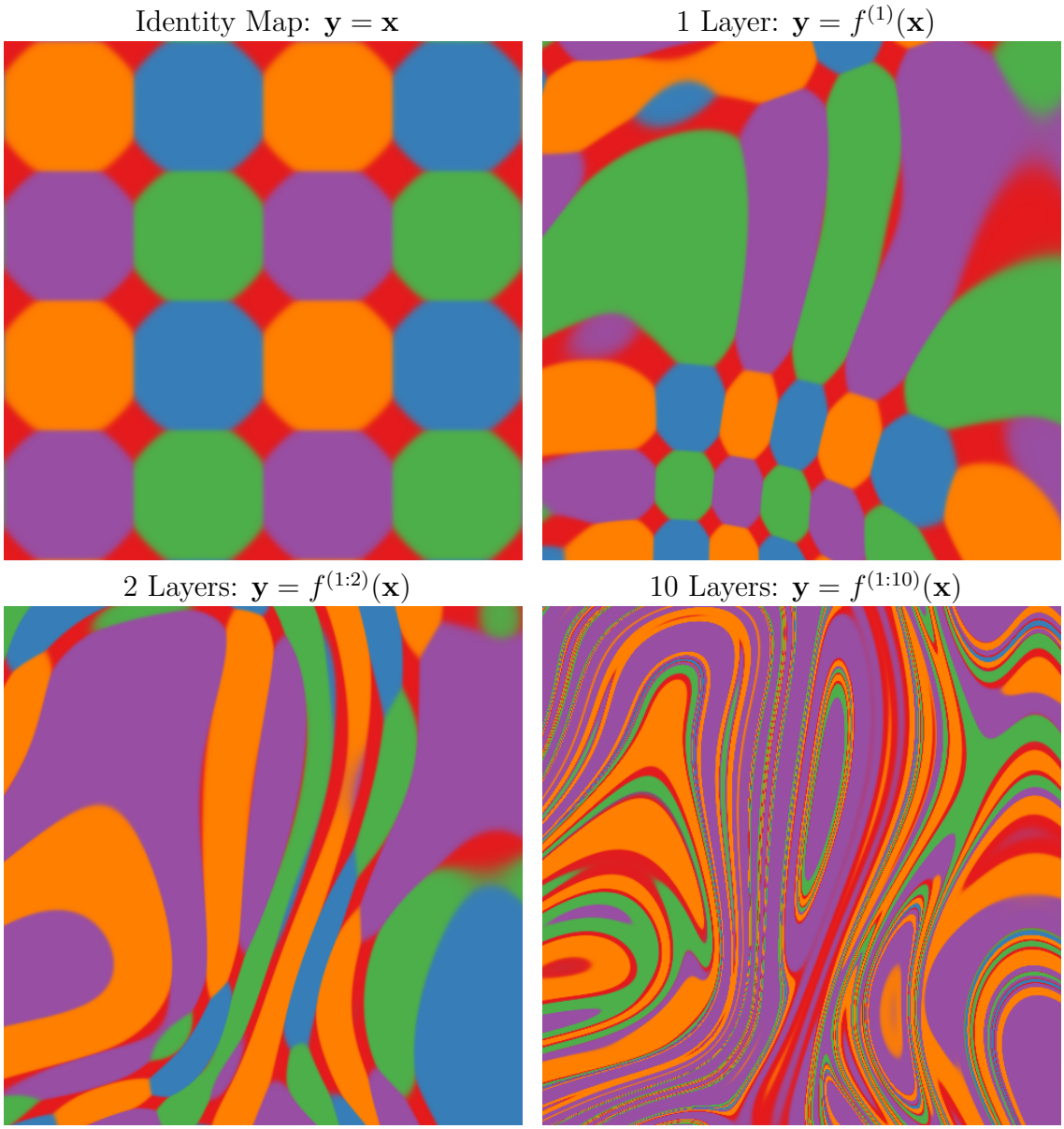

Fig. B.6 Feature mapping of a deep GP. Colors correspond to the location $\mathbf{y} = \mathbf{f}(\mathbf{x})$ that each point is mapped to after being warped by a deep GP. The number of directions in which the color changes rapidly corresponds to the number of large singular values in the Jacobian. Just as the densities in figure A.5 became locally one-dimensional, there is usually only one direction that one can move $\mathbf{x}$ in locally to change $\mathbf{y}$. This means that $\mathbf{f}$ is unlikely to be a suitable representation for decision tasks that depend on more than one aspect of $\mathbf{x}$.

tures. Similar connections between non-adjacent layers can also be found the primate visual cortex (Maunsell and van Essen, 1983). Formally, this functional dependence can

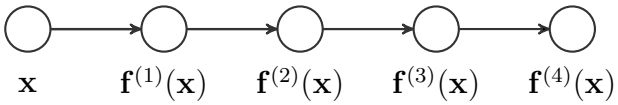

a) The standard MLP connectivity architecture.

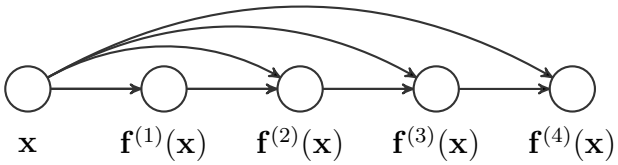

b) Input-connected architecture.

Fig. B.7 Two different architectures for deep neural networks. The standard architecture connects each layer's outputs to the next layer's inputs. The input-connected architecture also connects the original input $\mathbf{x}$ to each layer.

be written as

$$\mathbf{f}^{(1:L)}(\mathbf{x}) = \mathbf{f}^{(L)}\left(\mathbf{f}^{(1:L-1)}(\mathbf{x}), \mathbf{x}\right), \quad \forall L \tag{B.16}$$

Draws from the resulting prior are shown in figures A.8, A.9 and A.11. The Jacobian of the composed, input-connected deep function is defined by the recurrence

$$J^{1:L}(\mathbf{x}) = J^{L}\begin{bmatrix} J^{1:L-1} \\ I_D \end{bmatrix}. \tag{B.17}$$

Figure A.10 shows that with this architecture, even 50-layer deep gps have well-behaved singular value spectra.

B.6 Deep kernels

Bengio et al. (2006b) showed that kernel machines have limited generalization ability when they use a local kernel such as the squared-exp. However, many interesting non-local kernels can be constructed which allow non-trivial extrapolation. For example, periodic kernels can be viewed as a 2-layer-deep kernel, in which the first layer maps $x \to [\sin(x), \cos(x)]$, and the second layer maps through basis functions corresponding to the SE kernel.

Can we construct other useful kernels by composing fixed feature maps several times, creating deep kernels? Cho (2012) constructed kernels of this form, repeatedly applying

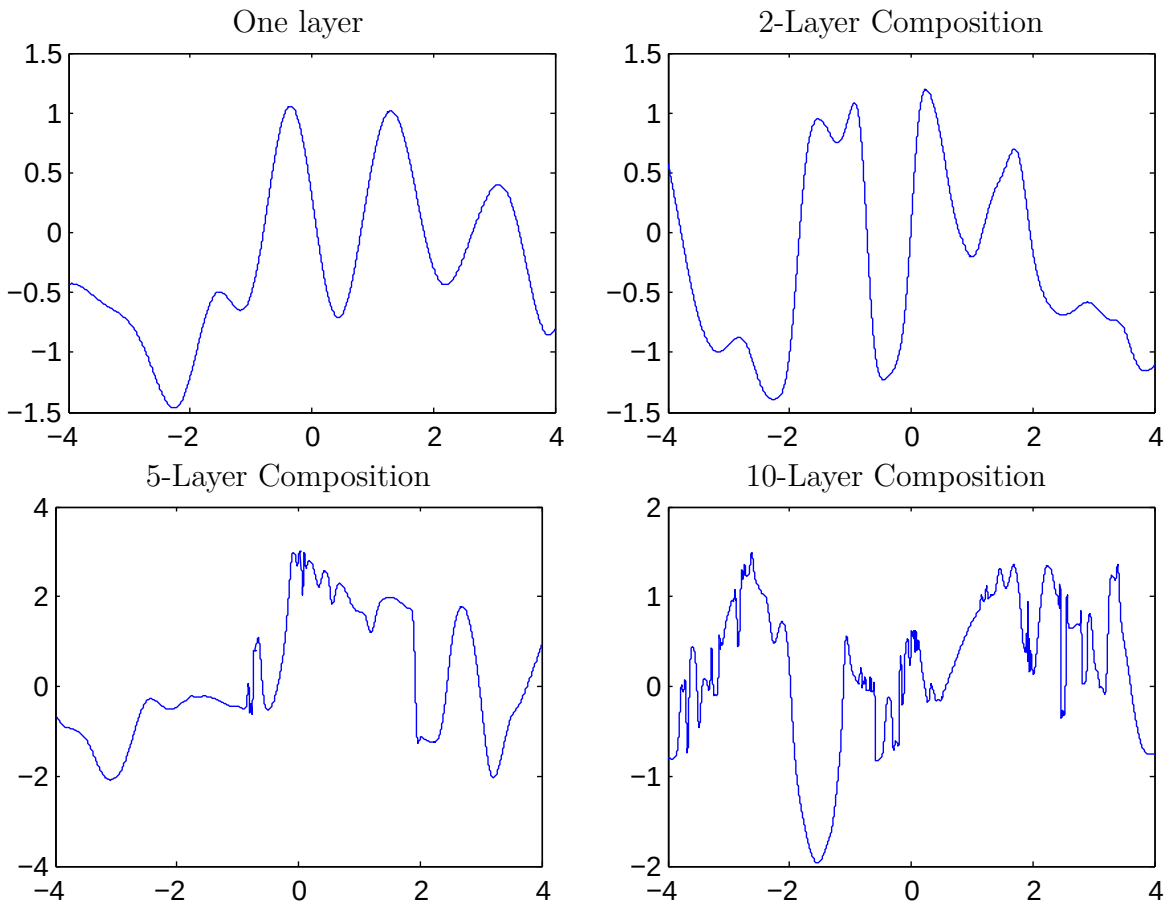

Fig. B.8 Draws from a 1D deep GP prior with each layer connected to the input. Even after many layers, the functions remain smooth in some regions, while varying rapidly in other regions. Compare to standard-connectivity deep GP draws shown in figure A.2.

multiple layers of feature mappings. We can compose the feature mapping of two kernels:

$$k_1(\mathbf{x}, \mathbf{x}') = \mathbf{h}_1(\mathbf{x})^\mathsf{T} \mathbf{h}_1(\mathbf{x}') \tag{B.18}$$

$$k_2(\mathbf{x}, \mathbf{x}') = \mathbf{h}_2(\mathbf{x})^\mathsf{T} \mathbf{h}_2(\mathbf{x}') \tag{B.19}$$

$$(k_1 \circ k_2)(\mathbf{x}, \mathbf{x}') = k_2(\mathbf{h}_1(\mathbf{x}), \mathbf{h}_1(\mathbf{x}')) \tag{B.20}$$

$$= [\mathbf{h}_2(\mathbf{h}_1(\mathbf{x}))]^\mathsf{T} \mathbf{h}_2(\mathbf{h}_1(\mathbf{x}')) \tag{B.21}$$

Composing the squared-exp kernel with any implicit mapping $\mathbf{h}(\mathbf{x})$ has a simple

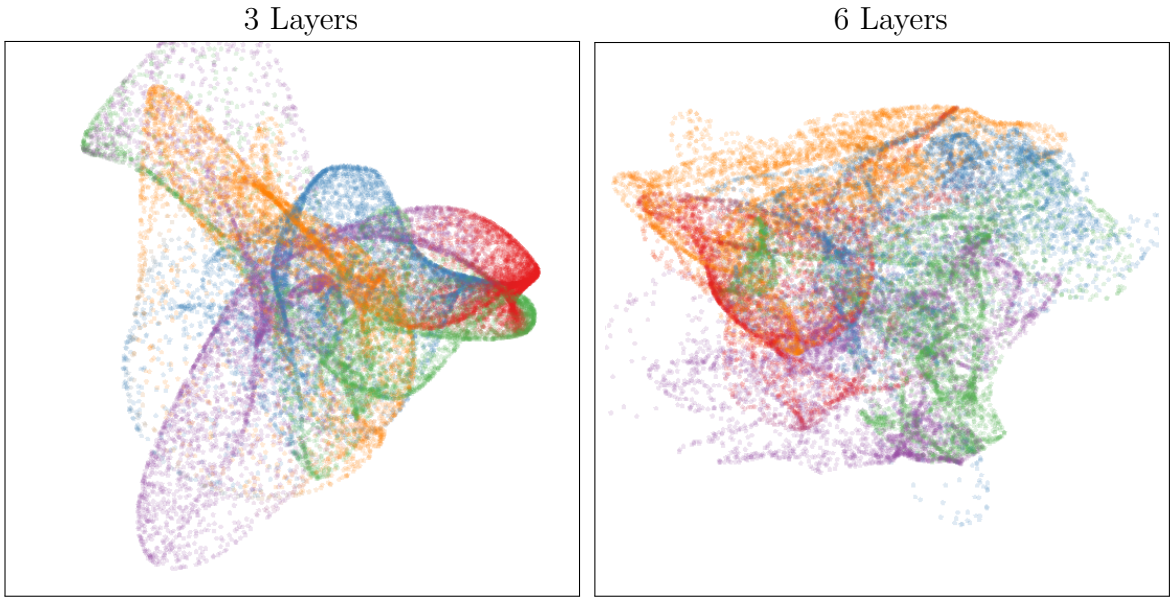

Fig. B.9 Left: Densities defined by a draw from a deep GP, with each layer connected to the input $\mathbf{x}$. As depth increases, the density becomes more complex without concentrating along filaments.

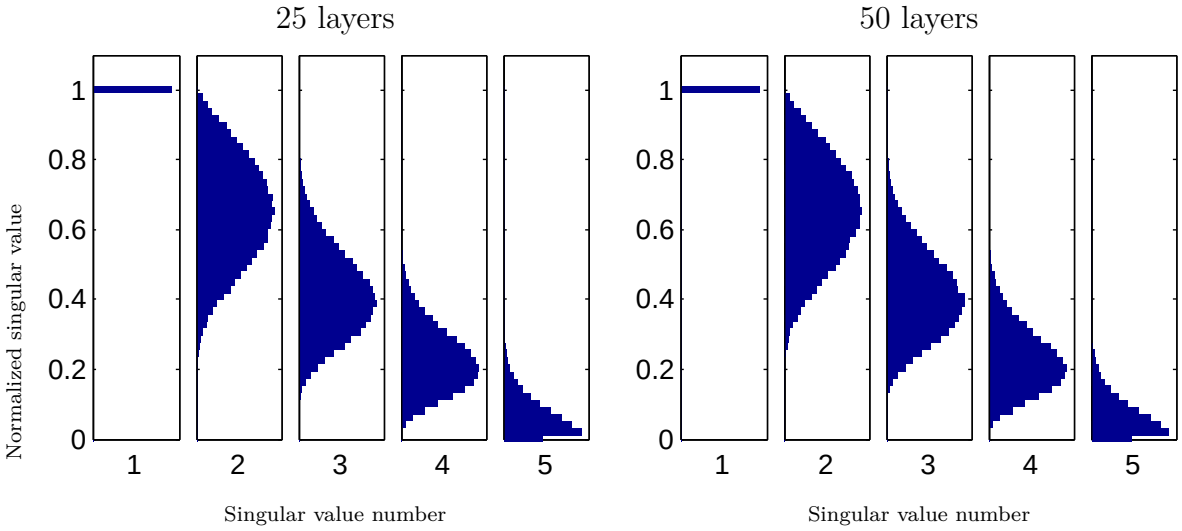

Fig. B.10 The distribution of singular values drawn from 5-dimensional input-connected deep GP priors 25 and 50 layers deep. The singular values remain roughly the same scale as one another.

closed form:

$$
\begin{aligned}
&k_{L+1}\left(\mathbf{x}, \mathbf{x}'\right) = k_{SE}\left(\mathbf{h}(\mathbf{x}), \mathbf{h}(\mathbf{x}')\right) = \\
&= \exp\left(-\frac{1}{2}||\mathbf{h}(\mathbf{x}) - \mathbf{h}(\mathbf{x}')||_2^2\right) \\
&= \exp\left(-\frac{1}{2}\left[\mathbf{h}(\mathbf{x})^\mathsf{T}\mathbf{h}(\mathbf{x}) - 2\mathbf{h}(\mathbf{x})^\mathsf{T}\mathbf{h}(\mathbf{x}') + \mathbf{h}(\mathbf{x}')^\mathsf{T}\mathbf{h}(\mathbf{x}')\right]\right) \\
&= \exp\left(-\frac{1}{2}\left[k_L(\mathbf{x}, \mathbf{x}) - 2k_L(\mathbf{x}, \mathbf{x}') + k_L(\mathbf{x}', \mathbf{x}')\right]\right)
\end{aligned}
\tag{B.22}
$$

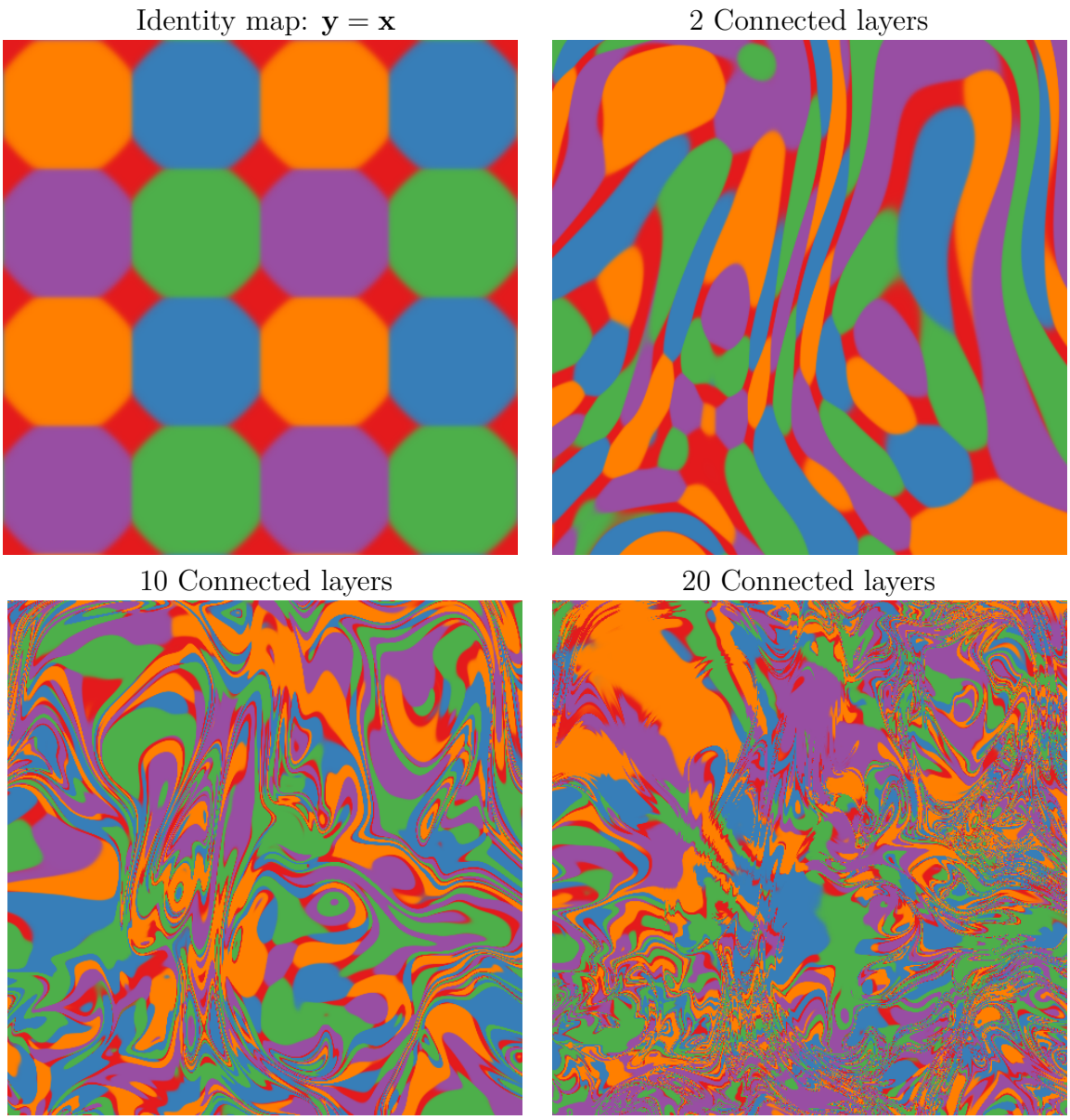

Fig. B.11 Feature mapping of a deep GP with each layer connected to the input $\mathbf{x}$. Just as the densities in figure A.9 remained locally two-dimensional even after many transformations, in this mapping there are often two directions that one can move locally in $\mathbf{x}$ to in order to change the values of $\mathbf{f}(\mathbf{x})$. This means that the prior puts mass on representations which sometimes depend on all aspects of the input. Compare to figure A.6.

Thus, we can express k_{L+1} exactly in terms of k_L.

Infinitely deep kernels What happens when we repeat this composition of feature maps many times, starting with the squared-exp kernel? In the infinite limit, this recursion converges to $k(\mathbf{x}, \mathbf{x}') = 1$ for all pairs of inputs, which corresponds to a prior on constant functions $f(\mathbf{x}) = c$.

A non-degenerate construction As before, we can overcome this degeneracy by connecting the inputs $\mathbf{x}$ to each layer. To do so, we simply augment the feature vector $\mathbf{h}_L(\mathbf{x})$ with $\mathbf{x}$ at each layer:

$$\begin{aligned} k_{L+1}(\mathbf{x}, \mathbf{x}') &= \exp\left(-\frac{1}{2}\left|\left|\begin{bmatrix}\mathbf{h}_L(\mathbf{x}) \\ \mathbf{x}\end{bmatrix} - \begin{bmatrix}\mathbf{h}_L(\mathbf{x}') \\ \mathbf{x}'\end{bmatrix}\right|\right|_2^2\right) \\ &= \exp\Big(-\frac{1}{2}\big[k_L(\mathbf{x}, \mathbf{x}) - 2k_L(\mathbf{x}, \mathbf{x}') \\ &\qquad + k_L(\mathbf{x}', \mathbf{x}') - ||\mathbf{x} - \mathbf{x}'||_2^2\big]\Big) \end{aligned} \tag{B.23}$$

For the SE kernel, this repeated mapping satisfies

$$k_\infty(\mathbf{x}, \mathbf{x}') - \log\left(k_\infty(\mathbf{x}, \mathbf{x}')\right) = 1 + \frac{1}{2}||\mathbf{x} - \mathbf{x}'||_2^2 \tag{B.24}$$

The solution to this recurrence has no closed form, but has a similar shape to the Ornstein-Uhlenbeck covariance $k_{\text{OU}}(x, x') = \exp(-|x - x'|)$ with lighter tails. Samples from a GP prior with this kernel are not differentiable, and are locally fractal.

B.6.1 When are deep kernels useful models?

Kernels correspond to fixed feature maps, and so kernel learning is an example of implicit representation learning. Such feature maps can capture rich structure (Duvenaud et al., 2013), and can enable many types of generalization, such as translation and rotation invariance in images (Kondor, 2008). Salakhutdinov and Hinton (2008) used a deep neural network to learn feature transforms for kernels, which learn invariances in an unsupervised manner. The relatively uninteresting properties of the kernels derived in this section simply reflect the fact that an arbitrary deep computation is not usually a useful representation, unless combined with learning.

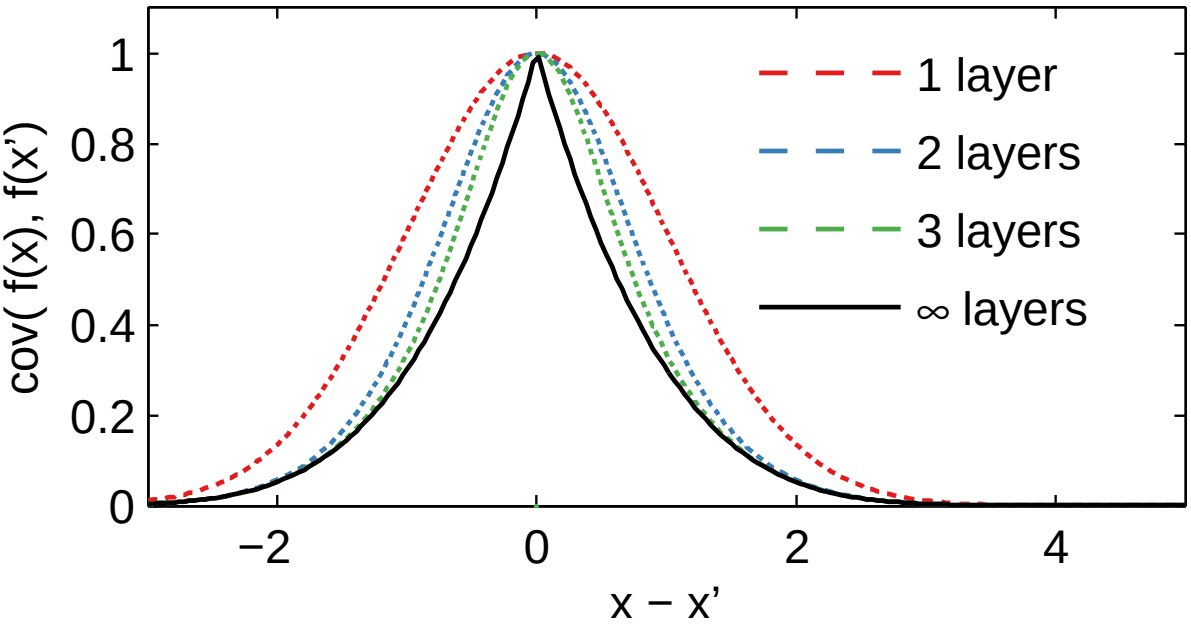

Fig. B.12 Input-connected deep kernels. By connecting the inputs $\mathbf{x}$ to each layer, the kernel can still depend on its input even after arbitrarily many layers of computation.

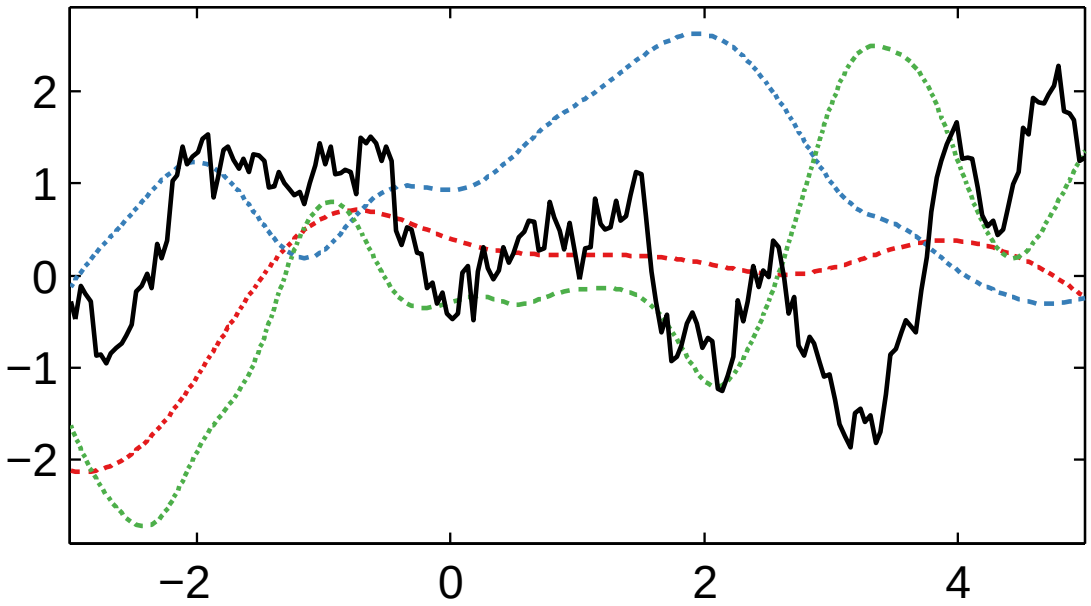

Fig. B.13 GP draws using deep input-connected kernels.

B.7 Dropout in Gaussian processes

Dropout is a method for regularizing neural networks (Hinton et al., 2012; Srivastava, 2013). Training with dropout entails randomly and independently "dropping" (setting to zero) some proportion p of features or inputs, in order to improve the robustness of the resulting network by reducing co-dependence between neurons. To maintain similar overall activation levels, weights are multiplied by $1/p$ at test time. Alternatively, feature activations are multiplied by $1/p$ during training. At test time, the set of models defined by all possible ways of dropping-out neurons is averaged over, usually in an approximate way.

Baldi and Sadowski (2013) and Wang and Manning (2013) analyzed dropout in terms of the effective prior induced by this procedure in several models, such as linear and logistic regression. In this section, we examine the priors on functions that result from performing dropout in the one-hidden-layer neural network implicitly defined by a gp (equation (A.4)).

B.7.1 Dropout on feature activations

First, we examine the prior that results from randomly dropping features from $\mathbf{h}(\mathbf{x})$ with probability p. If these features have a weight distribution with finite moments $\mathbb{E}[\alpha_i] = \mu, \mathbb{V}[\alpha_i] = \sigma^2$, then the distribution of weights after each one has been dropped out with probability p is:

$$r_i \overset{\text{iid}}{\sim} \text{Ber}(p) \qquad \mathbb{E}[r_i\alpha_i] = p\mu, \mathbb{V}[r_i\alpha_i] = p^2\sigma^2 \; . \tag{B.25}$$

However, after we increase the remaining activations to maintain the same expected activation by multiplying them by $1/p$, the resulting moments are again:

$$\mathbb{E}\left[\frac{1}{p}r_i\alpha_i\right] = \frac{p}{p}\mu = \mu, \quad \mathbb{V}\left[\frac{1}{p}r_i\alpha_i\right] = \frac{p^2}{p^2}\sigma^2 = \sigma^2 \; . \tag{B.26}$$

Thus, dropping out features of an infinitely-wide MLP does not change the model at all, since no individual feature can have more than infinitesimal contribution to the network output.

B.7.2 Dropping out inputs

In a gp with kernel $k(\mathbf{x}, \mathbf{x}') = \prod_{d=1}^{D} k_d(\mathbf{x}_d, \mathbf{x}'_d)$, exact averaging over all possible ways of dropping out inputs with probability $1/2$ results in a mixture of gps, each depending on only a subset of the inputs:

$$p\left(f(\mathbf{x})\right) = \frac{1}{2^D} \sum_{\mathbf{r} \in \{0,1\}^D} \mathrm{gp}\left(0, \prod_{d=1}^{D} k_d(\mathbf{x}_d, \mathbf{x}'_d)^{r_d}\right) \tag{B.27}$$

We present two results ways to gain intuition about this model.

First, if the kernel on each dimension has the form $k_d(\mathbf{x}_d, \mathbf{x}'_d) = g\left(\frac{\mathbf{x}_d - \mathbf{x}'_d}{w_d}\right)$, as does the SE kernel (A.10), then any input dimension can be dropped out by setting its lengthscale w_d to ∞. Thus, dropout on the inputs of a gp corresponds to a spike-and-slab prior on lengthscales, with each dimension independently having $w_d = \infty$ with probability $1/2$.

Another way to understand the resulting prior is to note that the dropout mixture (A.27) has the same covariance as

$$f(\mathbf{x}) \sim \mathrm{gp}\left(0, \frac{1}{2^{-2D}} \sum_{\mathbf{r} \in \{0,1\}^D} \prod_{d=1}^{D} k_d(\mathbf{x}_d, \mathbf{x}'_d)^{r_d}\right) \tag{B.28}$$

A gp whose covariance is a sum of kernels corresponds to a sum of functions, each distributed according to a gp. Therefore, (A.28) describes a sum of 2^D functions, each depending on a different subset of the inputs. This model class was studied by Duvenaud et al. (2011), who showed that exact inference in these models can be performed in $\mathcal{O}(N^2D^2 + N^3)$.

B.8 Related work

Deep gps were first proposed by Lawrence and Moore (2007). Variational inference in deep gps was developed by Damianou and Lawrence (2013), who also analyzed the effect of automatic relevance determination in that model.

Adams et al. (2010) proposed a prior on deep Bayesian networks. Their architecture has no connections except between adjacent layers, and may also be expected to have similar pathologies as deep gps as the number of layers increases. Deep Density Networks (Rippel and Adams, 2013) were constructed with invertibility in mind, with penalty terms encouraging the preservation of information about lower layers. Such priors are a promising approach to alleviating the pathology discussed in this paper.

Recurrent networks Bengio et al. (1994) and Pascanu et al. (2012) analyze a related problem with gradient-based learning in recurrent nets, the "exploding-gradients" problem. Hermans and Schrauwen (2012) analyze deep kernels corresponding to recurrent neural networks.

Analysis of deep learning Montavon et al. (2010) perform a layer-wise analysis of deep networks, and note that the performance of MLPs degrades as the number of layers with random weights increases. The importance of network architectures relative to learning has been examined by Saxe et al. (2011). Saxe et al. (2013) looked at the dynamics of learning in deep linear models, as a tractable approximation to deep neural networks.

B.9 Conclusions

In this work, we attempted to gain insight into the properties of deep neural networks by characterizing the sorts of functions likeley to be obtained under different choices of priors on compositions of functions.

First, we identified deep Gaussian processes as an easy-to-analyze model corresponding to multi-layer preceptrons with nonparametric activation functions. We then showed that representations based on repeated composition of independent functions exhibit a pathology where the representations becomes invariant to all directions of variation but one. Finally, we showed that this problem could be alleviated by connecting the input to each layer.

We also examined properties of deep kernels, corresponding to arbitrarily many compositions of fixed features. Finally, we derived models obtained by performing dropout on Gaussian processes, finding a tractable approximation to exact dropout in gps.

References

Ryan P Adams, Hanna M Wallach, and Zoubin Ghahramani. Learning the structure of deep sparse graphical models. In *International Conference on Artificial Intelligence and Statistics*, pages 1–8, 2010. (page 66)

Francis Bach. High-dimensional non-linear variable selection through hierarchical kernel learning. *CoRR*, abs/0909.0844, 2009. (pages 14, 19, 20, 23, and 25)

Pierre Baldi and Peter J Sadowski. Understanding dropout. In *Advances in Neural Information Processing Systems*, pages 2814–2822, 2013. (page 65)

Y. Bengio, O. Delalleau, and N. Le Roux. The curse of highly variable functions for local kernel machines. *Advances in neural information processing systems*, 18:107, 2006a. ISSN 1049-5258. (page 21)

Yoshua Bengio, Patrice Simard, and Paolo Frasconi. Learning long-term dependencies with gradient descent is difficult. *Neural Networks, IEEE Transactions on*, 5(2):157–166, 1994. (page 67)

Yoshua Bengio, Olivier Delalleau, and Nicolas Le Roux. The curse of highly variable functions for local kernel machines. pages 107–114, 2006b. (page 59)

Youngmin Cho. *Kernel methods for deep learning*. PhD thesis, University of California, San Diego, 2012. (page 59)

M. Christoudias, R. Urtasun, and T. Darrell. Bayesian localized multiple kernel learning. 2009. (pages 19 and 35)

Andreas Damianou and Neil Lawrence. Deep Gaussian processes. In *Artificial Intelligence and Statistics*, pages 207–215, 2013. (pages 48 and 66)

David Duvenaud, Hannes Nickisch, and Carl Edward Rasmussen. Additive Gaussian processes. In *Advances in Neural Information Processing Systems 24*, pages 226–234, Granada, Spain, 2011. (pages 35, 39, and 66)

David Duvenaud, James Robert Lloyd, Roger Grosse, Joshua B. Tenenbaum, and Zoubin Ghahramani. Structure discovery in nonparametric regression through compositional kernel search. In *Proceedings of the 30th International Conference on Machine Learning*, June 2013. (page 63)

Robert Gens and Pedro Domingos. Learning the structure of sum-product networks. In *International Conference on Machine learning*, 2013. (page 47)

T.J. Hastie and R.J. Tibshirani. *Generalized additive models*. Chapman & Hall/CRC, 1990. (pages 13 and 31)

Michiel Hermans and Benjamin Schrauwen. Recurrent kernel machines: Computing with infinite echo state networks. *Neural Computation*, 24(1):104–133, 2012. (page 67)

Geoffrey E Hinton, Nitish Srivastava, Alex Krizhevsky, Ilya Sutskever, and Ruslan R Salakhutdinov. Improving neural networks by preventing co-adaptation of feature detectors. *arXiv preprint arXiv:1207.0580*, 2012. (page 65)

C.G. Kaufman and S.R. Sain. Bayesian functional anova modeling using gaussian process prior distributions. *Bayesian Analysis*, 5(1):123–150, 2010. (page 19)

Imre Risi Kondor. *Group theoretical methods in machine learning*. PhD thesis, Columbia University, 2008. (page 63)

Neil D Lawrence and Andrew J Moore. Hierarchical Gaussian process latent variable models. In *Proceedings of the 24th international conference on Machine learning*, pages 481–488. ACM, 2007. (page 66)

Honglak Lee, Chaitanya Ekanadham, and Andrew Ng. Sparse deep belief net model for visual area v2. In *Advances in neural information processing systems*, pages 873–880, 2007. (page 47)

I.G. Macdonald. *Symmetric functions and Hall polynomials*. Oxford University Press, USA, 1998. ISBN 0198504500. (page 18)

James Martens. Deep learning via Hessian-free optimization. In *Proceedings of the 27th International Conference on Machine Learning*, pages 735–742, 2010. (page 47)

JH Maunsell and David C van Essen. The connections of the middle temporal visual area (mt) and their relationship to a cortical hierarchy in the macaque monkey. *The Journal of neuroscience*, 3(12):2563–2586, 1983. (page 58)

T.P. Minka. Expectation propagation for approximate bayesian inference. In *Uncertainty in Artificial Intelligence*, volume 17, pages 362–369. Citeseer, 2001. (page 23)

Grégoire Montavon, Dr Braun, and Klaus-Robert Müller. Layer-wise analysis of deep networks with Gaussian kernels. *Advances in Neural Information Processing Systems*, 23:1678–1686, 2010. (page 67)

Radford M Neal. *Bayesian learning for neural networks*. PhD thesis, University of Toronto, 1995. (pages 49 and 57)

J.A. Nelder and R.W.M. Wedderburn. Generalized linear models. *Journal of the Royal Statistical Society. Series A (General)*, 135(3):370–384, 1972. (page 13)

J. Nocedal. Updating quasi-newton matrices with limited storage. *Mathematics of computation*, 35(151):773–782, 1980. (page 23)

Razvan Pascanu, Tomas Mikolov, and Yoshua Bengio. Understanding the exploding gradient problem. *arXiv preprint arXiv:1211.5063*, 2012. (page 67)

T.A. Plate. Accuracy versus interpretability in flexible modeling: Implementing a tradeoff using gaussian process models. *Behaviormetrika*, 26:29–50, 1999. ISSN 0385-7417. (pages 17, 19, and 35)

C.E. Rasmussen and CKI Williams. Gaussian Processes for Machine Learning. *The MIT Press, Cambridge, MA, USA*, 2006. (pages 5, 14, 29, 31, and 37)

Salah Rifai, Grégoire Mesnil, Pascal Vincent, Xavier Muller, Yoshua Bengio, Yann Dauphin, and Xavier Glorot. Higher order contractive auto-encoder. In *Machine Learning and Knowledge Discovery in Databases*, pages 645–660. Springer, 2011a. (page 55)

Salah Rifai, Pascal Vincent, Xavier Muller, Xavier Glorot, and Yoshua Bengio. Contractive auto-encoders: Explicit invariance during feature extraction. In *Proceedings of the 28th International Conference on Machine Learning*, pages 833–840, 2011b. (page 55)

Oren Rippel and Ryan Prescott Adams. High-dimensional probability estimation with deep density models. *arXiv preprint arXiv:1302.5125*, 2013. (page 66)

Ruslan Salakhutdinov and Geoffrey Hinton. Using deep belief nets to learn covariance kernels for Gaussian processes. In *Advances in Neural Information Processing Systems*, volume 20, 2008. (page 63)

Andrew Saxe, Pang W Koh, Zhenghao Chen, Maneesh Bhand, Bipin Suresh, and Andrew Y Ng. On random weights and unsupervised feature learning. In *Proceedings of the 28th International Conference on Machine Learning (ICML-11)*, pages 1089–1096, 2011. (page 67)

Andrew M Saxe, James L McClelland, and Surya Ganguli. Dynamics of learning in deep linear neural networks. 2013. (page 67)

J. Shawe-Taylor and N. Cristianini. *Kernel methods for pattern analysis*. Cambridge University Press, 2004. ISBN 0521813972. (pages 27 and 28)

Ercan Solak, Roderick Murray-Smith, E. Solak, William Leithead, Carl Rasmussen, and Douglas Leith. Derivative observations in Gaussian process models of dynamic systems, 2003. (page 54)

Nitish Srivastava. *Improving neural networks with dropout*. PhD thesis, University of Toronto, 2013. (page 65)

R.P. Stanley. *Enumerative combinatorics*. Cambridge University Press, 2001. ISBN 0521789877. (page 18)

M. Stitson, A. Gammerman, V. Vapnik, V. Vovk, C. Watkins, and J. Weston. Support vector regression with ANOVA decomposition kernels. *Advances in kernel methods—Support vector learning*, pages 285–292, 1999. (page 20)

V.N. Vapnik. *Statistical learning theory*, volume 2. Wiley New York, 1998. (page 20)

G. Wahba. *Spline models for observational data*. Society for Industrial Mathematics, 1990. ISBN 0898712440. (pages 13, 21, and 35)

Sida Wang and Christopher Manning. Fast dropout training. In *Proceedings of the 30th International Conference on Machine Learning (ICML-13)*, pages 118–126, 2013. (page 65)